

A composite FeOOH@microalgae for heavy metals and Congo red removal from aqueous solution

Junjun Wang^{a,b}, Juan Huang^c, Meiyang Xu^d, Zhanfei Li^{a,b}, Ling Fan^{a,b}, Ran Chen^{a,b}, Weimin Zeng^{a,b,e}, Xueling Wu^{a,b}, Jiaokun Li^{a,b,f}, Runlan Yu^{a,b}, Yuandong Liu^{a,b}, Li Shen^{a,b,*}

^aSchool of Minerals Processing and Bioengineering, Central South University, Changsha – 410083, China, Tel./Fax: +86-731-8879815; emails: lishen@csu.edu.cn (L. Shen), 1784082260@qq.com (J. Wang), 1654351012@qq.com (Z. Li), 1098786348@qq.com (L. Fan), 1395317471@qq.com (R. Chen), zengweimin1024@126.com (W. Zeng), wxlcsu@csu.edu.cn (X. Wu), lijiaokun@csu.edu.cn (J. Li), yrl715@sina.com (R. Yu), 438320852@qq.com (Y. Liu)

^bKey Laboratory of Biometallurgy, Ministry of Education, Changsha – 410083, China

^cMaterials Science and Engineering, Central South University, Changsha – 410083, China, email: 309993163@qq.com (J. Huang)

^dState Key Laboratory of Applied Microbiology in South China, Guangdong Institute of Microbiology, Guangdong – 510070, China, email: xumy@gdim.cn (M. Xu)

^eThe Commonwealth Scientific and Industrial Research Organization (CSIRO) Process Science and Engineering, Clayton, Victoria, Australia

^fSchool of Metallurgy and Environment, Central South University, Changsha – 410083, China

Received 16 August 2019; Accepted 3 February 2020

ABSTRACT

A microalgae-oxide complex (FeOOH@Microalgae) was successfully synthesized; it showed a high adsorption ability for removal of Cr(VI), Cu(II), Pb(II), Cd(II), and Congo red from contaminated aqueous solution. The product was characterized using X-ray diffraction, scanning electron microscopy (SEM), transmission electron micrography (TEM), X-ray photoelectron spectroscopy, and Fourier-transform infrared spectroscopy. The SEM and TEM images showed that the complex formed using nano-sized FeOOH, which covered micron-sized microalgae, and the degree of product aggregation was related to the synthetic temperature. The aggregation degree increased with a decrease in the synthesis temperature, thus, micron-sized microalgae can be immobilized. The adsorption experimental results of pH effect, sorption kinetics, and the isotherm indicated that FeOOH@Microalgae showed a reasonable adsorption effect on four metal ions, and the adsorption ability of Pb(II) was substantially higher than that of the other three ions. Kinetic data showed agreement with a pseudo-second-order equation, and the Langmuir model fit the isotherm data of four heavy metal ions. The adsorption mechanism indicated that the adsorption process was related to the surface hydroxyl (or carboxyl) groups of the adsorbent that interacted with metal ions. Hence, FeOOH@Microalgae, as an efficient adsorbent, can be extensively applied for the treatment of heavy metal contaminated wastewater.

Keywords: *Synechocystis* sp. PCC6803; Hydroxyl iron oxide (FeOOH); Water treatment; Heavy-metal ions; Adsorption

* Corresponding author.

1. Introduction

The intensification of social modernization processes has resulted in the great pollution of the living environment [1,2]. For example, water pollution and soil pollution [3], especially due to heavy metals [4], is a serious threat to human survival [5,6]. Among the various kinds of heavy metals, Cr(VI), Cu(II), Pb(II), and Cd(II) are more serious due to their high toxicity and negligible biodegradability [7–10]. The bioaccumulation of these metals, beyond a permissible quantity, can cause various diseases, even cancer [11–13]. Thus, the removal of heavy metal ions from water is critical, the protection of human health and the environment must be prioritized [14,15].

Many technologies exist to remove heavy metal ions from polluted aqueous solution, including physical and chemical methods [16–21]. However, these methods have various shortcomings, such as high cost, low removal rate, laborious techniques, and even secondary pollution [22,23]. Conversely, adsorption has attracted extensive research attention due to its simple operation and low cost [24,25], including numerous adsorbents for heavy metal removal from wastewater [26,27]. Recently, several reports have addressed the application of metal oxide materials in the treatment of heavy-metal pollution [28,29] due to their affinity and selectivity in the adsorption process. In addition, microalgae are a potentially biological adsorbent that can remove heavy metals from contaminated aqueous solution [30–32]. The surface hydroxyl and carboxyl groups of microalgae can interact with metal ions [33]. Dead microalgae also show excellent adsorption ability. However, research about the combination of materials and biological adsorbents are seldom reported. In this study, with different reaction temperatures, a compound adsorbent was formed by combining metal oxides and microalgae, which had the advantages of metal oxides and microalgae to overcome these limitations and treat heavy metal contaminated wastewater.

The main contents of this study are listed as follows: (i) the preparation of the compound adsorbent via microalgae covering metal oxides at different reaction temperatures (70°C, 60°C, and 50°C), respectively, (ii) the characterization of product by X-ray power diffraction (XRD), Fourier transform infrared spectroscopy (FT-IR), scanning electron microscopy (SEM), transmission electron microscopy (TEM), and X-ray photoelectron spectroscopy (XPS), (iii) the investigation of the sorption kinetics and isotherms of the compound adsorbent, and (iv) the study of adsorption mechanisms.

2. Materials and methods

2.1. Synthesis of the materials

The *Synechocystis* sp. PCC6803 was inoculated in the sterilized BG-11 medium and cultured at 30°C, pH 7.1, light intensity of 2,000 lx and light-dark ratio of 12:12 h [34]. The bottles were shake twice a day to prevent agglomeration [35]. After 6 d in these conditions, the culture was centrifuged at 10,000 rpm for 10 min to harvest the microalgae cells. The washed cells were lyophilized and then ground into powder.

In a typical procedure, FeCl₃ (0.243 g) and *Synechocystis* sp. PCC6803 powder (0.05 g) was dissolved in 35 mL of

distilled water with urea (0.25 g). After stirring for 30 min, the reaction solution was poured into a Teflon-lined autoclave. The autoclave was sealed and placed at one of three different reaction temperatures (70°C, 60°C, and 50°C) for 6 h. After the reaction, the precipitate was collected by centrifugation, washed three times with ethanol and deionized water, and then dried at 70°C for 6 h.

2.2. Characteristic analysis

The products before and after adsorption were characterized by the following techniques. Crystal phases of the material were identified using a D/max-2400 XRD meter (Rigaku, Japan) at 100 kV and 40 mA, with Cu K α radiation ($k = 1.542 \text{ \AA}$) and a scanning rate of 4°min⁻¹. The surface morphology and structure were examined with SEM, and an energy dispersive X-ray (EDX) microanalysis was performed using the ZEISS DSM-960 microscope (Germany) equipped with an EDX unit. A high-resolution image was observed by the TecnaiG2 F20 S-TWIN TMP transmission electron microscopy (America). The FT-IR spectra an Bruker Vertex 70 FT-IR spectrophotometer instrument (Germany) in the 400–4,000 cm⁻¹ range.

2.3. Adsorption experiments

The different concentrations of Cr(VI), Cu(II), Pb(II), and Cd(II) were prepared using K₂Cr₂O₇, Cu(NO₃)₂, Pb(NO₃)₂, and CdCl₂, respectively. The effect of pH (2.0–8.0) on the adsorption ability of FeOOH@Microalgae on different metal ions was investigated. For the adsorption kinetics study, 80 mg of FeOOH@Microalgae was added to 100 mL solution (initial ion concentration of 80 mg L⁻¹). The concentration was measured by sampling at a specific time (5, 10, 20, 30, 60, 90, 120, 150, 180, and 240 min). For the adsorption isotherms, 80 mg of the FeOOH@Microalgae was added to 100 mL solutions with different initial ion concentrations (10, 20, 50, 100, 200, and 500 mg L⁻¹, respectively). Simultaneously, *Synechocystis* sp. PCC6803 and FeOOH were used as control groups. After stirring for 3 h at room temperature, the supernatant was separated and measured by inductively coupled plasma (ICP).

2.4. Removal of an organic pollutant

Congo red (C₃₂H₂₂N₆O₆S₂Na₂), which is an azo dye, was utilized as an organic water pollutant [36]. The FeOOH@Microalgae (0.02 g) was mixed with 20 mL of Congo red solution (initial concentration 50 mg L⁻¹). Simultaneously, microalgae and FeOOH were used as control groups. The supernatant was separated at 10,000 rpm for 5 min at different adsorption time, and analyzed at 300–650 cm⁻¹ wavelength by ultraviolet-visible spectroscopy (Shimadzu, model 2550).

2.5. Effects of co-existing cation

The effects of four common coexisting ions (K⁺, Na⁺, Mg²⁺, and Ca²⁺) on FeOOH@Microalgae adsorption behavior were investigated in single-metal systems (Cr(VI)/Cu(II)/Pb(II)/Cd(II)). The experiment was performed in the following conditions: metal ion concentration: 40 mg/L,

coexistence ion concentration: 0.01 mol/L, adsorption dose: 1.0 g/L, pH: 3.0 for Cr(VI), pH: 5.0 for Cu(II)/Pb(II)/Cd(II), adsorption temperature: 30°C. After 60 min of oscillating adsorption, the concentration of ions (Cr(VI)/Cu(II)/Pb(II)/Cd(II)) was determined by ICP in the solution. All adsorption experiments were performed in triplicate.

3. Results and discussion

3.1. Characterization of the product

3.1.1. XRD analysis

The chemical composition of the synthesized product was analyzed using XRD measurement. As shown in Fig. 1a, the diffraction peaks from different reaction temperatures were consistent with the recorded values of FeOOH [Joint Committee on Powder Diffraction Standards (JCPDS) 75–1594]. The sharp diffraction peaks in the spectra indicated that the prepared products exhibited satisfactory crystal form. The following formation mechanism was proposed (Fig. 4). FeOOH was obtained by hydrothermal reaction of FeCl₃ with urea in aqueous solution, as described in Eqs. (1) and (2), which was similar to the synthesis of FeOOH discussed by Gou et al. [37].

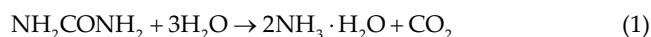


Fig. 1a shows that the impurity peaks of the product synthesized at 50°C were less detected than that at 70°C and 60°C. This finding indicated that the lower reaction temperature can guarantee the synthesis of FeOOH. The main reason for the destruction of microalgae structure was the higher synthesis temperature. With a decrease in the reaction temperature, the intensity of the characteristic peaks was not distinctly weakened but the intensity of the impurity peaks can be distinctly reduced, which suggested that the decrease in reaction temperature can not only ensure the formation of FeOOH but also maintain the

complete structure of microalgae, which provided a base for synthesizing FeOOH. This finding also revealed that 5°C was the optimal synthesis temperature, which not only enabled successful formation of FeOOH on the surface of microalgae but also protected the microalgae structure, and therefore, caused excessive number of peaks. Thus, the FeOOH synthesized at 50°C was selected to investigate the adsorption kinetics and isotherms of different metal ions.

3.1.2. FTIR analysis

To further study the composition of functional groups of synthetic products, Fourier infrared spectrum analysis was performed as shown in Fig. 1b. The infrared spectrums of the products synthesized at the different temperatures had identical functional group compositions. The functional groups of products are summarized in Table 1. The spectra at 3,417; 1,651; 1,538; 1,446; 1,236; 1,154; 1,028; 838; and 669 cm⁻¹ were attributed to O–H stretching [38], C=C, and C=O stretching vibrations of the hydrocarbon, carbonyl moieties on the material surface [39], protonated amine (–NH₃⁺), C–H stretch bending of CH₂ group [40], C–C skeleton vibration [41], –CO stretch of COOH [42], the characteristic band of CH–O–CH₂ [43], and bending modes of aromatic compounds [44], respectively. The main difference of the products and microalgae was the band at 672 cm⁻¹, which can be assigned to the absorption peak of FeOOH [45], indicating the synthesis of FeOOH in the product. Compared with the microalgal functional groups, the products not only retained the characteristic functional groups of microalgae, which played key roles in adsorbing metal ions but also had unique group composition (e.g., Fe–O). The synthetic product, which had functional groups of individual microalgae and FeOOH, was a complex. This result indicated that the different synthesis temperatures did not affect the functional group species but could impact the intensity of the characteristic peaks.

3.1.3. XPS analysis

The previous analysis has shown the existence of FeOOH in the product. XPS spectra were employed to

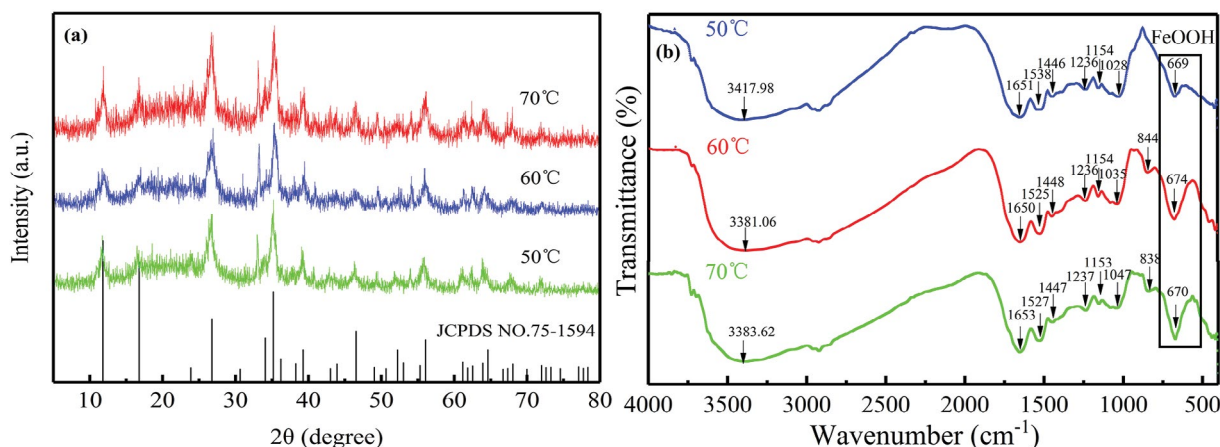


Fig. 1. (a) XRD patterns and (b) FTIR spectra of the FeOOH@Microalgae obtained at different reaction temperatures (70°C, 60°C, and 50°C).

Table 1

Wavenumbers (cm^{-1}) of the FeOOH@Microalgae obtained at different reaction temperatures (70°C, 60°C, and 50°C) and microalgae

Material types	Functional groups						
	-OH	C=O	-NH ₃ ⁺	CH	-C-O-	CH-O-CH ₂	FeOOH
70°C	3,383	1,653	1,527	1,447	1,153	1,047	670
60°C	3,381	1,650	1,525	1,448	1,154	1,035	674
50°C	3,417	1,651	1,538	1,446	1,154	1,028	669
Microalgae	-OH	-CH ₂	-CONH-	-NH ₃ ⁺	CH	-C-O-	CH-O-CH ₂
	3,378	2,927	1,655	1,539	1,451	1,154	1,033

further analyze additional evidence of the existence of FeOOH (Fig. 2). The survey spectra showed that the main common elements of product were Fe, C, and O. The C element was the main element of microalgae, and the Fe element was the main element of FeOOH, which indicated that the synthesized product was a complex of FeOOH

and microalgae. According to high-resolution scanning (Figs. 2b–d), the percentages of Fe, C, and O atoms in the product ranged between those of microalgae and FeOOH, and the specific element content values can be obtained from Table 2, which further indicated that the product (FeOOH@Microalgae) was a complex of microalgae and FeOOH.

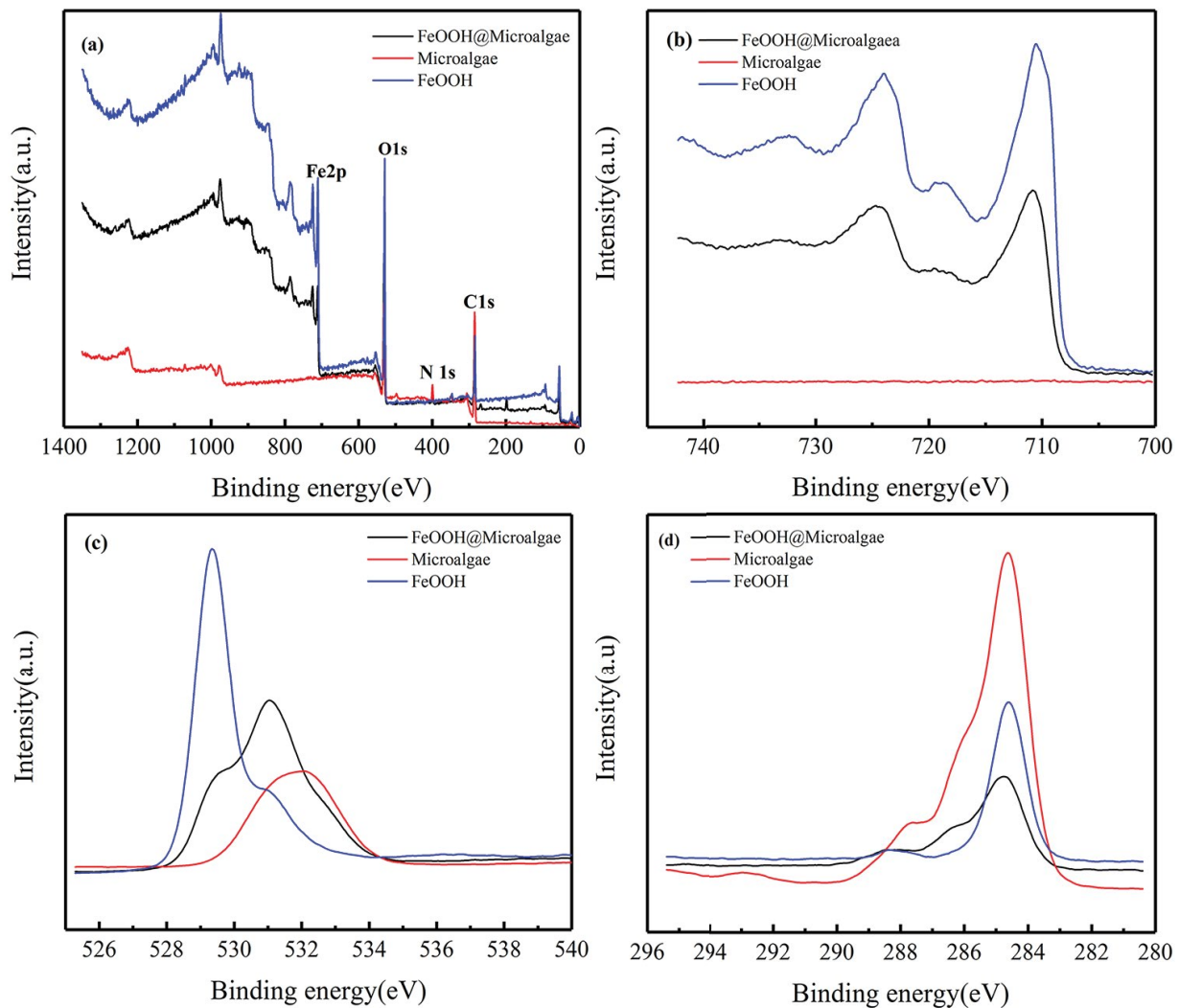


Fig. 2. XPS spectra for FeOOH@Microalgae, Microalgae and FeOOH, respectively. (a) Survey scans of the spectral region from 0 to 1,400 eV. (b–d) Represent high-resolution narrow scans of XPS Fe2p, O1s, and C1s, respectively, as a function of electron binding energy.

3.1.4. SEM analysis

SEM was used to study the morphology of products. Fig. 3 shows the surface morphology and spectrum analysis of the FeOOH@Microalgae synthesized at different reaction temperatures. As shown in Figs. 3a–c, the morphology of globular microalgae became more distinct with a decrease in the reaction temperature because the structure of microalgae was destroyed at higher temperature. Thus, the presence of spherical particles was not evident in the scanned image. Figs. 3c and c-1 present the product synthesized at 50°C, which showed spherical aggregates of approximately 2 μm and a further tendency to aggregate. Compared with Figs. 3c and c-1, the product synthesized at 70°C (Figs. 3a and a-1) exhibited an entirely different morphology with

no visible aggregation of micron particles. This finding indicated that the condition at 70°C completely destroyed structure of the microalgae considering that the higher temperatures can carbonize the microalgae and destroy its structure. At the intermediate temperature of 60°C (Figs. 3b and b-1), the images showed a distinct microalgae morphology; however, the spherical diameter increased and appeared scattered compared with Figs. 3c and c-1. This finding indicated that a large amount of FeOOH was synthesized to cover the surface of microalgae at this temperature but a considerable amount of debris suggested that the structure of the microalgae was damaged. In addition, spherical particles were relatively more dispersed and less aggregated, which showed that the synthetic temperature can affect the formation of FeOOH and the extent of damage to the microalgae structure, as well as the degree of aggregation. The high-resolution scanning of the product synthesized at 50°C in Figs. 3c-2–c-4 indicated that the nanoscale rod-like material covered the surface of the micron spherical particles. Via energy spectrum analysis, the composition of the rod-like products was determined as FeOOH, which indicated that the synthesized product has a composite structure formed by nanoscale rod-like FeOOH that covered the surface of the microalgae. The results showed that 50°C was the optimum synthesis temperature,

Table 2
Atomic percentage of elements of the FeOOH@Microalgae, microalgae, and FeOOH

Constituent	Fe atomic %	O atomic %	C atomic %
FeOOH@Microalgae	11.5	40.53	41.8
Microalgae	0.16	22.98	70.32
FeOOH	23.07	46.07	30.86

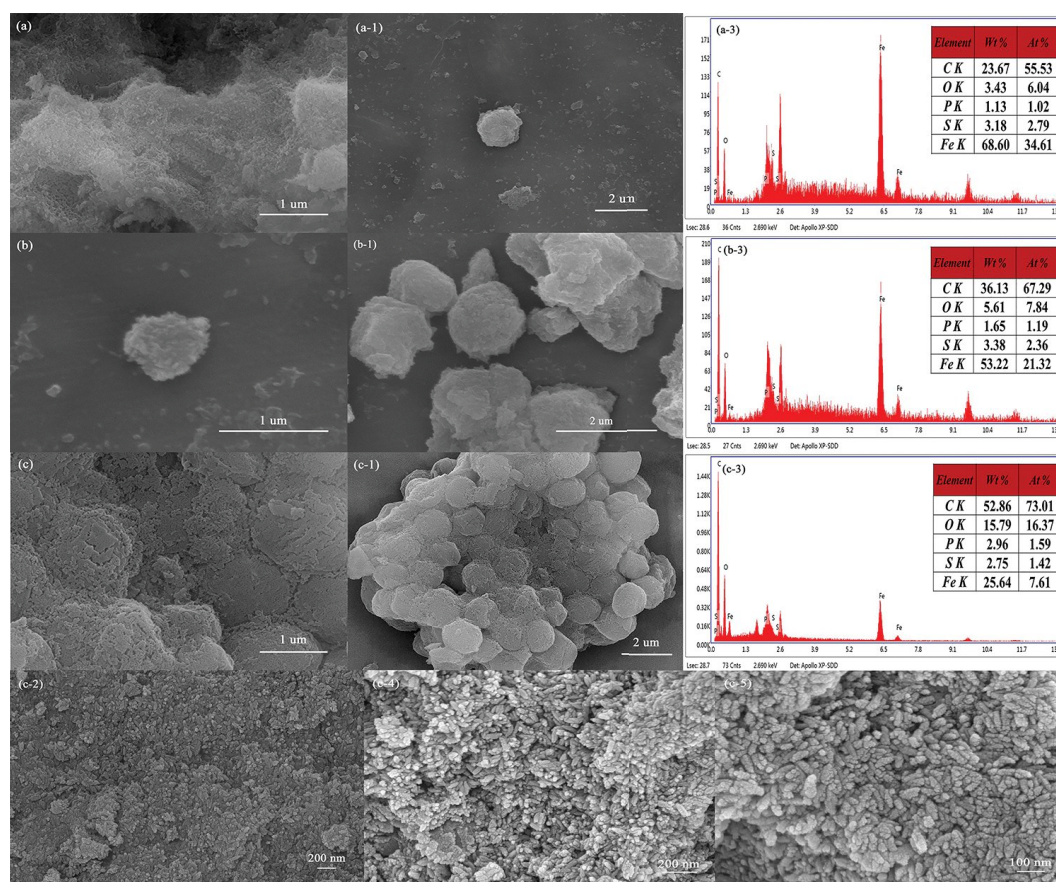


Fig. 3. SEM images and EDX spectra of the synthesized materials. (a), (a-1), (a-3); (b), (b-1), (b-3); and (c), (c-1), (c-3) represent the SEM images and EDX spectra of the synthesized FeOOH@Microalgae at different reaction temperatures (70°C, 60°C, and 50°C, respectively). (c-2), (c-4), and (c-5) represent the high-resolution scanning images of FeOOH@Microalgae.

which formed FeOOH on the surface of the microalgae and resulted in the lowest degree of damage to the microalgae, and the aggregation effect was distinct. The XPS analysis showed that the product was a complex of microalgae and FeOOH. The scanning observations and energy spectrum analysis suggested that the surface of the microalgae was covered with FeOOH. The analysis results were consistent with the characterization results of the XRD.

The element compositions of the products were obtained with EDX analysis, and the spectra are shown in Fig. 3. The results showed that S and P were the characteristic elements of the microalgae, while Fe and O were the major elements of FeOOH. As shown in Figs. 3a-3, b-3, c-3, the existence of four elements indicated that the product was composed of iron hydroxide and microalgae. Combined with SEM observation, the results showed that FeOOH covered the surface of the microalgae, and as the reaction temperature decreased, the carbon content of the synthesized product increased while the iron content decreased. The findings also indicated that the lower temperature affected the synthesis of FeOOH, while the microalgae were weakly damaged to maintain a complete structure. The previous XPS analysis revealed that the product was a complex of microalgae and FeOOH. The scanning observation and energy spectrum analysis suggested that the product consisted of a composite of FeOOH that coated the surface of the microalgae.

A possible formation mechanism was proposed (Fig. 4). Different synthesis temperatures can produce different structures of products. The synthesis temperature of 70°C enabled the synthesis of FeOOH but the structure of the microalgae has been completely destroyed, and micron spheres cannot be distinctly observed. The synthetic FeOOH was not coated with microalgae. Although the synthesis temperature of 60°C also guaranteed the synthesis of FeOOH and did not cause distinct damage to the microalgae structure, the micron spheres covered with FeOOH were not highly aggregated but relatively dispersed. The 50°C synthesis temperature can not only guarantee the synthesis

of FeOOH on the surface of the microalgae but also protect the structure of microalgae. A comparison revealed that 50°C was a better synthesis temperature for attaining the synthetic FeOOH that successfully covered the surface of microalgae and is highly aggregated.

3.1.5. TEM analysis

TEM was performed to further observe the product structure. Fig. 5 shows transmission photographs and energy spectra of the product synthesized at 50°C at different positions. The TEM analysis of the FeOOH@Microalgae (Figs. 5a and a-1) showed a uniform nano-rod shape with an average length of 100 nm and an average width of 25 nm. Moreover, the energy spectrum (Fig. 5a-1) shows high iron content, which indicated that most of the FeOOH was distributed on the surface. Nanorods tended to aggregate in the center of FeOOH@Microalgae (Fig. 5b). Compared with the surface layer of FeOOH@Microalgae (Figs. 5a and a-1), the carbon content significantly increased, while the iron content relatively decreased, which indicated that the central position was a complex of FeOOH and microalgae. However, a distinct structure is not visible in the interior (Fig. 5c). The low content of Fe indicated that the interior location mainly consisted of microalgae with high carbon content. This analysis suggested that the synthetic product was a complex of FeOOH and microalgae. FeOOH was mainly distributed on the surface, while microalgae inside the product were covered by nanorod FeOOH to immobilize the microalgae. The immobilizing effect was related to the synthesis temperature.

3.2. Adsorption experiments

3.2.1. Effect of pH on Cr(VI), Cu(II), Pb(II), and Cd(II)

The pH value substantially influences on the functional groups of the adsorbent and existence state of metal ions in the adsorption process [46,47]. The effect of solution pH on the adsorption capacity of heavy metal ions using FeOOH@

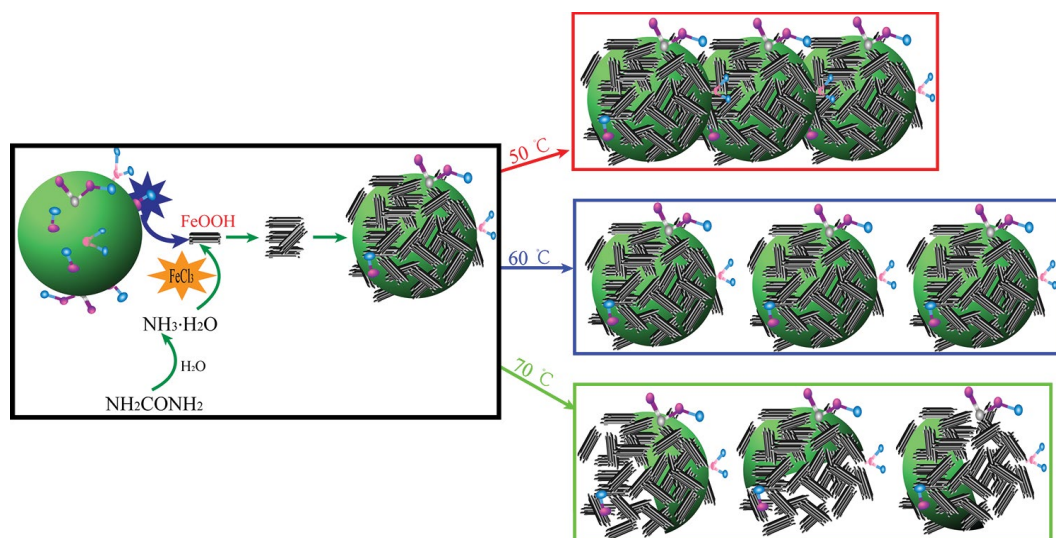


Fig. 4. Schematic of the formation mechanism of FeOOH@Microalgae.

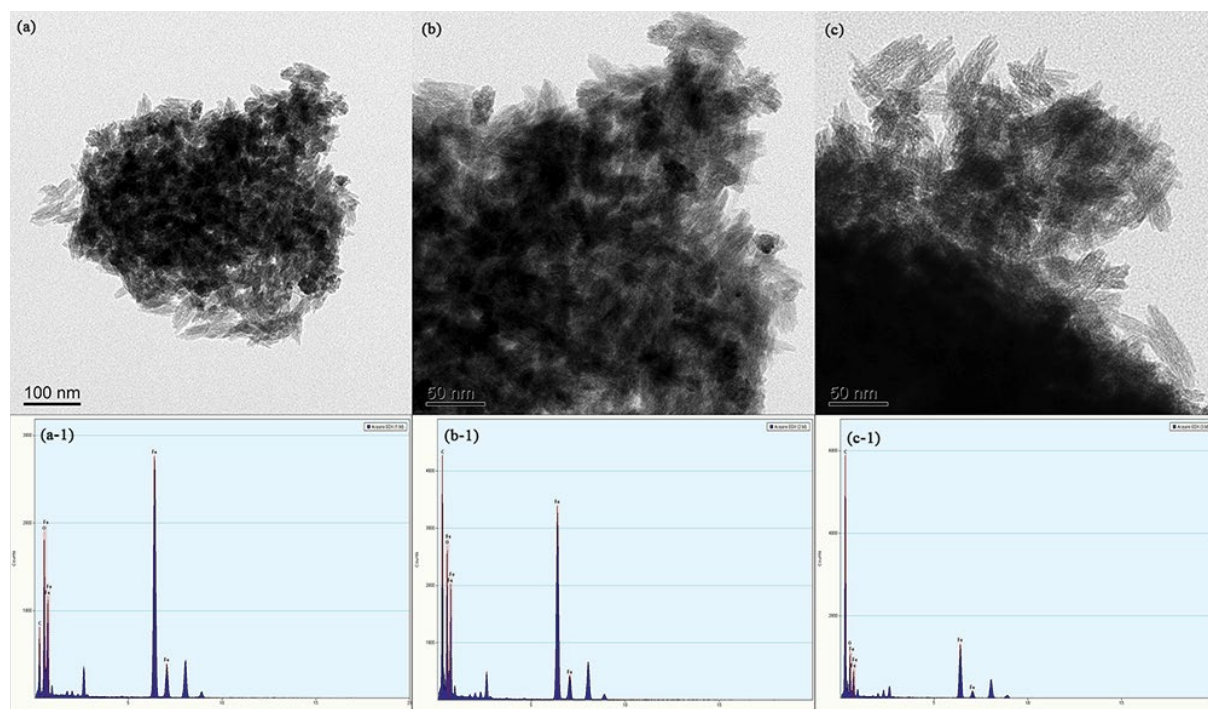
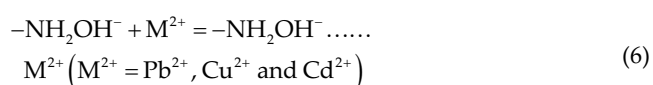
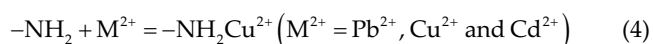


Fig. 5. TEM images of the synthesized FeOOH@Microalgae at 50°C. (a–c) TEM images and (a-1, b-1, and c-1) energy spectrum of exposed/intermediate/buried structure.

Microalgae was investigated at pH 2.0–8.0 (Fig. 6). As shown in Fig. 6, the influence of the pH values for Cu(II), Pb(II), and Cd(II) adsorption was nearly identical. The adsorption rate increased with an increase in pH value. The maximum adsorption was observed at pH 5.0–6.0. Cu(II), Pb(II), and Cd(II) are presented in Eqs. (3) and (6) at different pH values in the aqueous solution [48]. For example, in the adsorption process of Cu(II) [49], a large amount of NH_2 on the surface of the adsorbent was protonated within a low pH range [50], as shown in Eqs. (3), which was adverse to adsorption of Cu(II). However, with a gradual increase in pH, the protonation degree of NH_2 on the surface of the adsorbent decreased, and a substantial amount of NH_2 was released for the adsorption of Cu(II) (Eqs. (5) and (6)). Thus, the adsorption amount of Cu(II) increased, which indicated that electrostatic action had a major role in the adsorption process of Cu(II). The adsorption process of Pb(II) and Cd(II) were similar to that of Cu(II).



For the acidic condition, the main forms of Cr ions are HCrO_4^- , $\text{Cr}_2\text{O}_7^{2-}$, $\text{Cr}_2\text{O}_4^{2-}$, and $\text{Cr}_3\text{O}_{10}^{2-}$ in aqueous solution.

As shown in Fig. 6a, the removal of Cr ions was substantially affected by the pH value, and the maximum adsorption capacity was observed at pH 3.0. At a lower pH value, the adsorbent tended to be more protonated and preferred the dominant adsorption of HCrO_4^- ion [51,52]. With an increase in pH value, the degree of protonation decreased, and the competition between the hydroxyl group and the chromate caused a reduction in the adsorption effect. The adsorption effect of pH value on Cr(VI) was similar to the results reported in previous articles [53]. Baran et al. [53] investigated the effect of different initial pH (2.0–8.0) for the Cr(VI) adsorption effect on different adsorbents. The 10 mg adsorbent (chitin, chitosan, ion exchanges) was added to 10 mL of 100 mg/L Cr(VI) solution in the adsorption condition (200 rpm and 25°C), which showed that the pH 3.0 was optimal for chitin and chitosan. With the pH increase in the adsorption medium, Cr(VI) adsorption efficiency gradually increased until the optimal pH was attained. When the initial pH value was increased, Cr(VI) precipitation occurred due to the presence of a large number of $-\text{OH}$ in the adsorption media. At very low pH, the adsorbent surface was surrounded by a large number of hydronium ions, and Cr(VI) was mainly the anion of HCrO_4^- and $\text{Cr}_2\text{O}_7^{2-}$. These hydronium ions enhanced Cr(VI)'s interaction with the adsorbent binding site via greater attraction. As a result, the cause of the adsorption capacity difference of FeOOH@Microalgae by pH values was distinct.

3.2.2. Effects of co-existing cation

In general, industrial wastewater contains not only heavy metal ions, but also some inorganic cations (such as

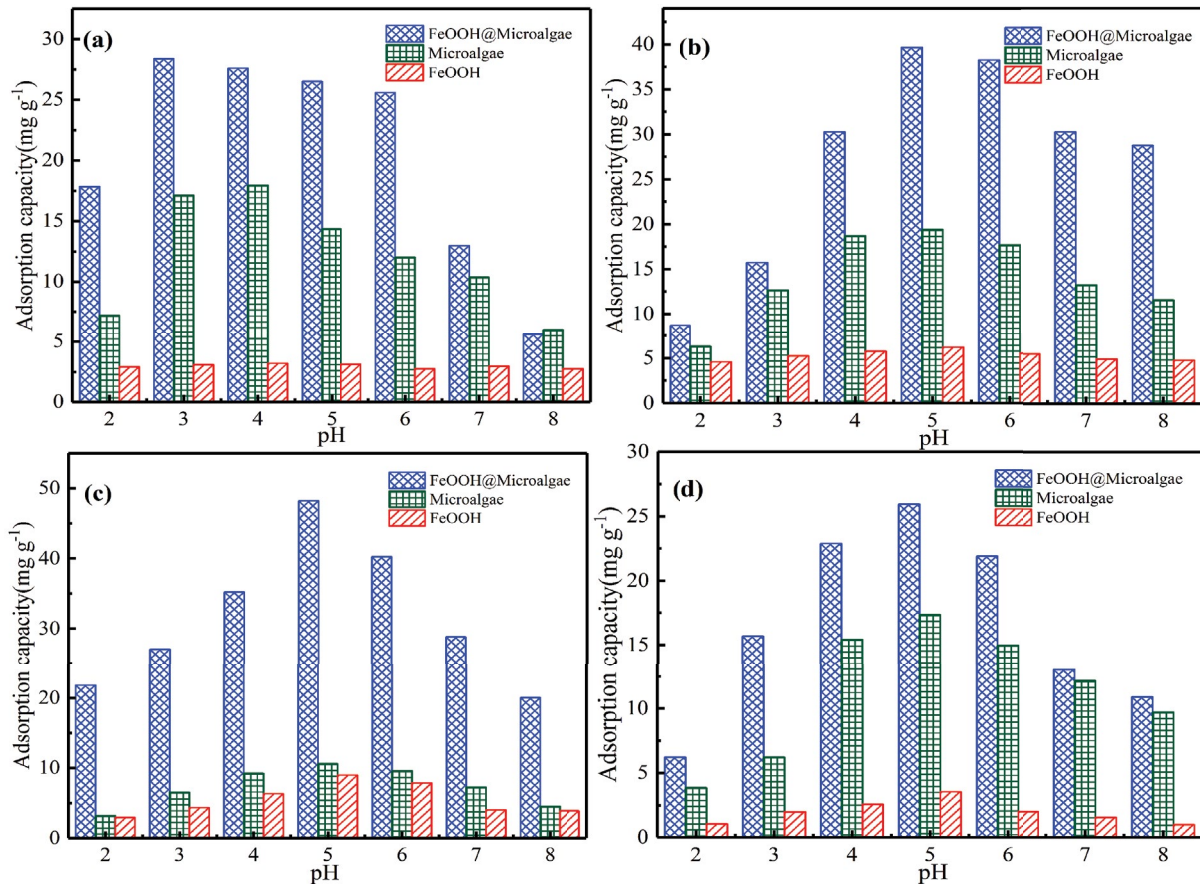


Fig. 6. Effect of pH on FeOOH@Microalgae adsorption of (a) Cr(VI), (b) Cu(II), (c) Pb(II), and (d) Cd(II) (initial concentration: 80 mg L⁻¹; adsorbent dose: 0.5 g L⁻¹; contact time: 6 h; temperature: 30°C).

K⁺, Na⁺, and Mg²⁺). In the adsorption process, the effects of these ions on the adsorption capacity of the adsorbents should be considered due to their competition for active sites [54,55]. Fig. 7 shows the effect of common cations on the adsorption capacity of FeOOH@Microalgae in a single metal system. The coexisting ions can decrease the adsorption efficiency of FeOOH@Microalgae to metal ions but the degree of decrease differed, in which Na⁺ had the least influence (<3%). This finding may be attributed to the competitive adsorption from coexisting ions, which indicated that the cation exchange mechanism had a role in the ion removal process. Note that the presence of 0.01 M ion strength was common in most practical wastewater systems. Although coexisting ions caused FeOOH@Microalgae to reduce the adsorption efficiency of metal ions, the reduction degree was relatively low (<10%). Therefore, FeOOH@Microalgae was advantageous to the removal of metal ions.

3.2.3. Effect of other metal other ions after adsorption of one metal ion

After FeOOH@Microalgae adsorbed one metal ion, the adsorption experiments of the remaining three ions were performed in the following conditions: adsorption dose of 1.0 g/L, temperature of 30°C, and initial ion concentration of 100 mg/L. The experimental results are shown in Fig. 8.

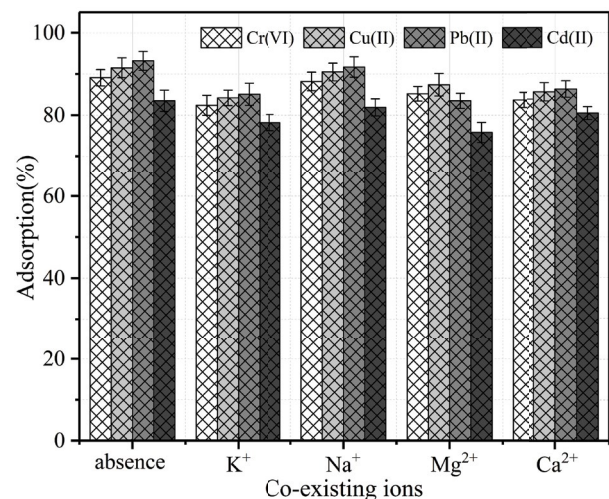


Fig. 7. Effects of co-existing salts on the adsorption of Cr(VI), Cu(II), Pb(II), and Cd(II).

The result indicated that the adsorption effect of other ions was distinctly reduced after the adsorption of one metal ion. The result may be contributed to the notion that the binding sites on the surface of the adsorbent were constant, and most

of the adsorption sites have been saturated after the adsorbent adsorbed one metal ion. For other ions, therefore, few empty sites remained. Another explanation was the existence of large structural groups near the residual adsorption sites to prevent the approach and binding of metal ions.

3.2.4. Adsorption kinetics

In the adsorption process, kinetics is a considerably important parameter for designing sorption systems and selecting the optimum operating conditions for the metals removal process [40,43]. The Lagergren-first-order model and pseudo-second-order model are generally expressed as Eqs. (7) and (8) [56]:

$$\ln(q_e - q_t) = \ln q_e - k_1 t \tag{7}$$

$$\frac{t}{q_t} = \frac{1}{k_2 q_e^2} + \frac{t}{q_e} \tag{8}$$

where q_e and q_t (mg g^{-1}) are the equilibrium amount adsorption capacity and dynamic (at time t) amount adsorption capacity, respectively, k_1 and k_2 are the rate constants of pseudo-first-order (min^{-1}) adsorption and pseudo-second-order ($\text{g mg}^{-1} \text{min}^{-1}$) adsorption, respectively.

Fig. 9 shows the adsorption effect of FeOOH@Microalgae for four metal ions. The adsorption capacity was rapidly enhanced at the initial time and then slowed and reached equilibrium. At room temperature, approximately 1 h was sufficient to attain adsorption equilibrium. The adsorption effects of FeOOH@Microalgae for four heavy metals were considerably higher than those of pure *Synechocystis* sp. PCC6803 and FeOOH. This finding indicated that the FeOOH@Microalgae had better adsorption capacity. FeOOH@Microalgae combined the advantages of FeOOH and Microalgae; several groups exist on the surface of Microalgae and FeOOH generally had a large specific surface area. FeOOH@Microalgae combined these advantages to enhance the adsorption capacity. Table 3 presents the k_1 , k_2 , and R^2 values of the two kinetic models. Compared with

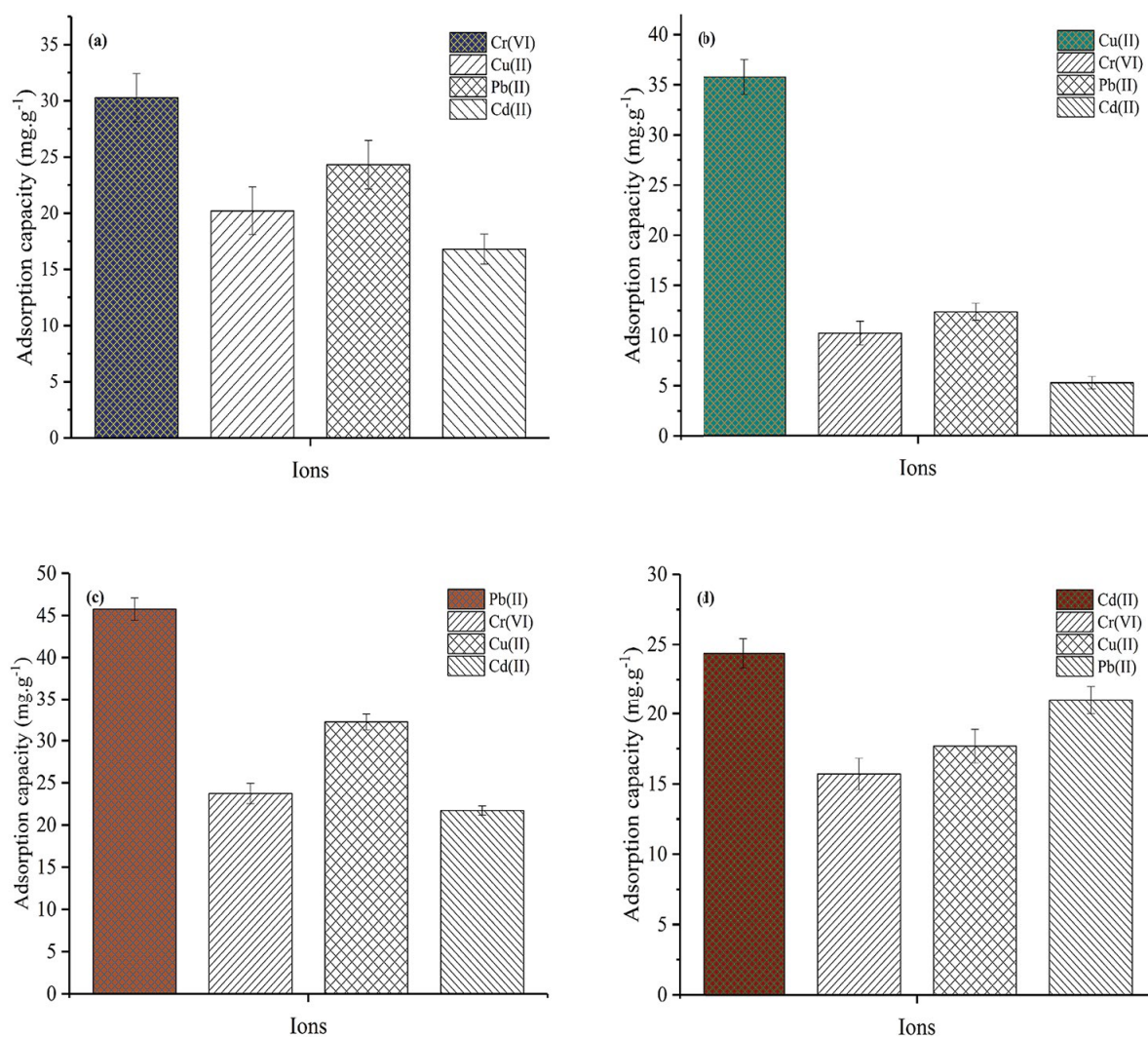


Fig. 8. Adsorption of three metal ions on FeOOH@Microalgae after adsorption of one metal ion. (a–d) represented the adsorption of other metals after adsorption of Cr(VI), Cu(II), Pb(II), and Cd(II), respectively.

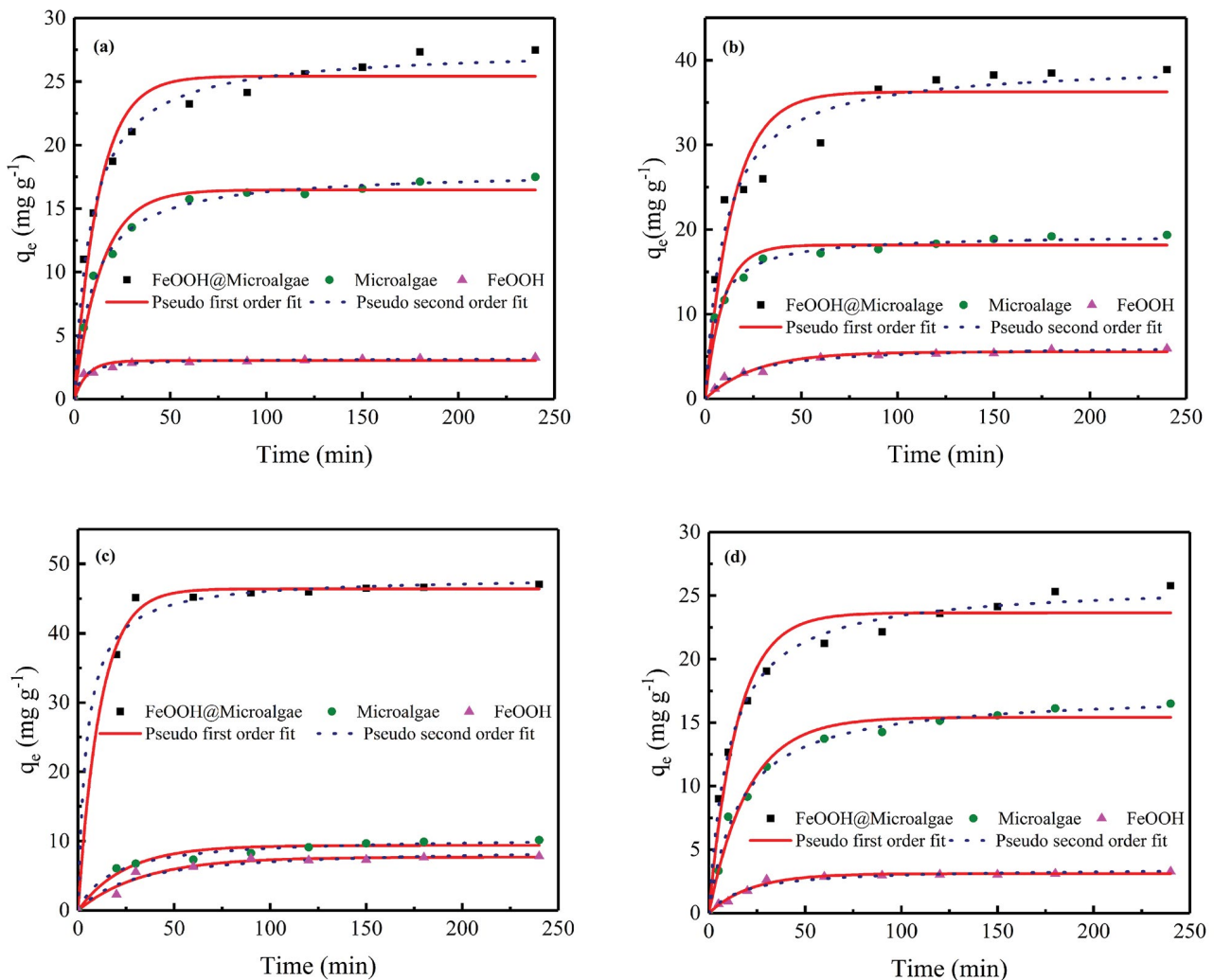


Fig. 9. Adsorption kinetic plots of the different heavy metal ions. (a–d) represent Cr(VI), Cu(II), Pb(II), and Cd(II), respectively, with the FeOOH@Microalgae (experiment conditions: initial Cr(VI), Cu(II), Pb(II), and Cd(II) concentration: 80 mg L⁻¹; adsorbent dose: 0.5 g L⁻¹; contact time: 6 h, solution pH: 3.0 for Cr(VI), 5.3 ± 0.1 for Cu(II)/Pb(II)/Cd(II); temperature: 30°C).

the pseudo-first-order model, the correlation coefficient values (R^2) of the adsorbents indicated a better fit of the pseudo-second-order equation with the experimental data. According to the pseudo-second-order equation, the calculated values (q_e) showed agreement with the experimental data of FeOOH@Microalgae. The results indicated that the adsorption of heavy metals on the adsorbents obeyed the pseudo-second-order kinetic, which suggested a chemisorption process [57].

In the pseudo-second-order model, the estimated equilibrium uptake (q_e) of the FeOOH@Microalgae values were 27.61 mg g⁻¹ for Cr(VI), 39.63 mg g⁻¹ for Cu(II), 48.17 mg g⁻¹ for Pb(II), and 25.93 mg g⁻¹ for Cd(II). The equilibrium rate constants (k_2) were 0.004 g mg⁻¹ min⁻¹ for Cr(VI), 0.004 g mg⁻¹ min⁻¹ for Cu(II), 0.005 g mg⁻¹ min⁻¹ for Pb(II), and 0.003 g mg⁻¹ min⁻¹ for Cd(II). These results confirmed that the FeOOH@Microalgae can selectively bind with different heavy metal ions. Compared with Cr(VI), Cu(II), and Cd(II), the FeOOH@Microalgae showed a better adsorption effect on Pb(II).

3.2.5. Equilibrium adsorption isotherms

Two typical isotherm models Langmuir and Freundlich isotherm were used to analyze the equilibrium data of the adsorption of four heavy-metal ions on FeOOH@Microalgae [40,43]. The Langmuir and Freundlich isotherm are expressed as Eqs. (5) and (6):

$$q_e = \frac{q_m K_L c_e}{1 + K_L c_e} \quad (9)$$

$$q_e = K_F c_e^{1/n} \quad (10)$$

where c_e (mg L⁻¹) is the equilibrium concentration of the total ion in the solution; q_e (mg g⁻¹) is the maximum adsorption capacity; K_L is the Langmuir constant; K_F is the Freundlich constant; and $1/n$ is the Freundlich empirical parameter, which represents the heterogeneity of the system.

Fig. 10 shows the adsorption Cr(VI), Cu(II), Pb(II), and Cd(II) for different initial concentrations. The

Table 3
Comparison of rate constants calculated based on the pseudo-first-order and pseudo-second-order models

Heavy metal	Lagergren-first-order model			Pseudo-second-order model		
	q_e (mg g ⁻¹)	k_1 (min ⁻¹)	R^2	q_e (mg g ⁻¹)	k_1 (mg g ⁻¹ min ⁻¹)	R^2
Cr(VI)						
FeOOH@Microalgae	25.427	0.079	0.961	27.611	0.004	0.993
Microalgae	16.472	0.071	0.980	17.949	0.006	0.995
FeOOH	3.032	0.148	0.944	3.203	0.076	0.984
Cu(II)						
FeOOH@Microalgae	36.257	0.069	0.916	39.628	0.004	0.967
Microalgae	18.168	0.107	0.964	19.397	0.008	0.994
FeOOH	5.546	0.038	0.964	6.333	0.008	0.983
Pb(II)						
FeOOH@Microalgae	46.419	0.087	0.990	48.168	0.005	0.991
Microalgae	9.386	0.041	0.949	10.578	0.005	0.982
FeOOH	7.681	0.029	0.956	9.047	0.004	0.941
Cd(II)						
FeOOH@Microalgae	23.644	0.068	0.965	25.932	0.003	0.994
Microalgae	15.418	0.049	0.979	17.347	0.004	0.994
FeOOH	3.114	0.046	0.984	3.537	0.056	0.973

calculated parameters are summarized in Table 4. According to the values of the correlation coefficients (R^2), the Langmuir model was more suitable than the Freundlich model ($R^2 = 0.601, 0.659, 0.663, \text{ and } 0.678$ for Cr(VI), Cu(II), Pb(II), and Cd(II), respectively, of the FeOOH@Microalgae) for describing the adsorption process. This finding suggested a homogeneous adsorption process of heavy metal ions on the sorbent when a heterogeneous adsorption was assumed, due to the diversity of the adsorption sites. The $1/n$ values of the sorption of Cr(VI), Cu(II), Pb(II), and Cd(II) on the FeOOH@Microalgae indicated that the sorption intensity was satisfactory (or favorable) at relatively high concentrations but substantially less at lower concentrations [58,59].

Based on this isotherm, the maximum adsorption capacities of the FeOOH@Microalgae were approximately 31.06 mg g⁻¹ for Cr(VI), 54.04 mg g⁻¹ for Pb(II), 40.63 mg g⁻¹ for Cu(II), and 30.83 mg g⁻¹ for Cd(II). These values were considerably higher than those of previously reported nano-materials [60–66]. The adsorption capacity at equilibrium was substantially higher than that of pure *Synechocystis* sp. PCC6803 and FeOOH, and approximately 10 times higher than that of FeOOH. The maximum adsorption capacities of various adsorbents previously reported for Cr(VI), Cu(II), Pb(II), and Cd(II) are summarized in Table 5. These results indicated that FeOOH@Microalgae showed a large adsorption capacity for Cr(VI), Cu(II), Pb(II), and Cd(II), indicating that it can be potentially employed as an excellent adsorbent for heavy metals in water treatment.

3.2.6. Adsorption capability for Congo red

To further investigate the advantages of FeOOH@Microalgae in water treatment, the adsorption experiment

about Congo red was performed. Fig. 11 showed the adsorption efficiency of Congo red solutions over time after treatment with FeOOH@Microalgae. FeOOH@Microalgae was capable of a removal efficiency of approximately 90% for Congo red. The maximum adsorption capacity of FeOOH@Microalgae for Congo red was calculated to be 96 mg g⁻¹. The removal efficiency was largely attributed to the composite structure of FeOOH and microalgae and the electrostatic attraction between the FeOOH@Microalgae and Congo red. The adsorption capabilities for Congo red (Fig. 8a), which is FeOOH@Microalgae > commercial FeOOH > *Synechocystis* sp. PCC6803 powder, indicated that combining FeOOH with microalgae can significantly improve the adsorption effect for Congo red. The result was also better than the previously reported adsorption capacities of some materials for Congo red [110].

3.3. Adsorption mechanism

3.3.1. FTIR analysis

To further confirm the adsorption mechanism of FeOOH@Microalgae, the changes of characteristic adsorption peaks in adsorbents before and after adsorption were investigated using FTIR. As shown in Fig. 12 and Table 6, before and after adsorption of heavy metals, the position, and shape of the characteristic peaks were substantially shifted. The O–H peak at 3417 cm⁻¹ for FeOOH@Microalgae was observed before adsorption, which was shifted to 3,292; 3,297; 3,285; and 3,273 cm⁻¹ after adsorption of Cr(VI), Cu(II), Pb(II), and Cd(II), respectively (Fig. 11a). The –CH₂ stretching vibration was at and 2,926 cm⁻¹, which was observed at 2,927; 2,927; 2,926; 2,921 cm⁻¹ after adsorption of four metal ions.

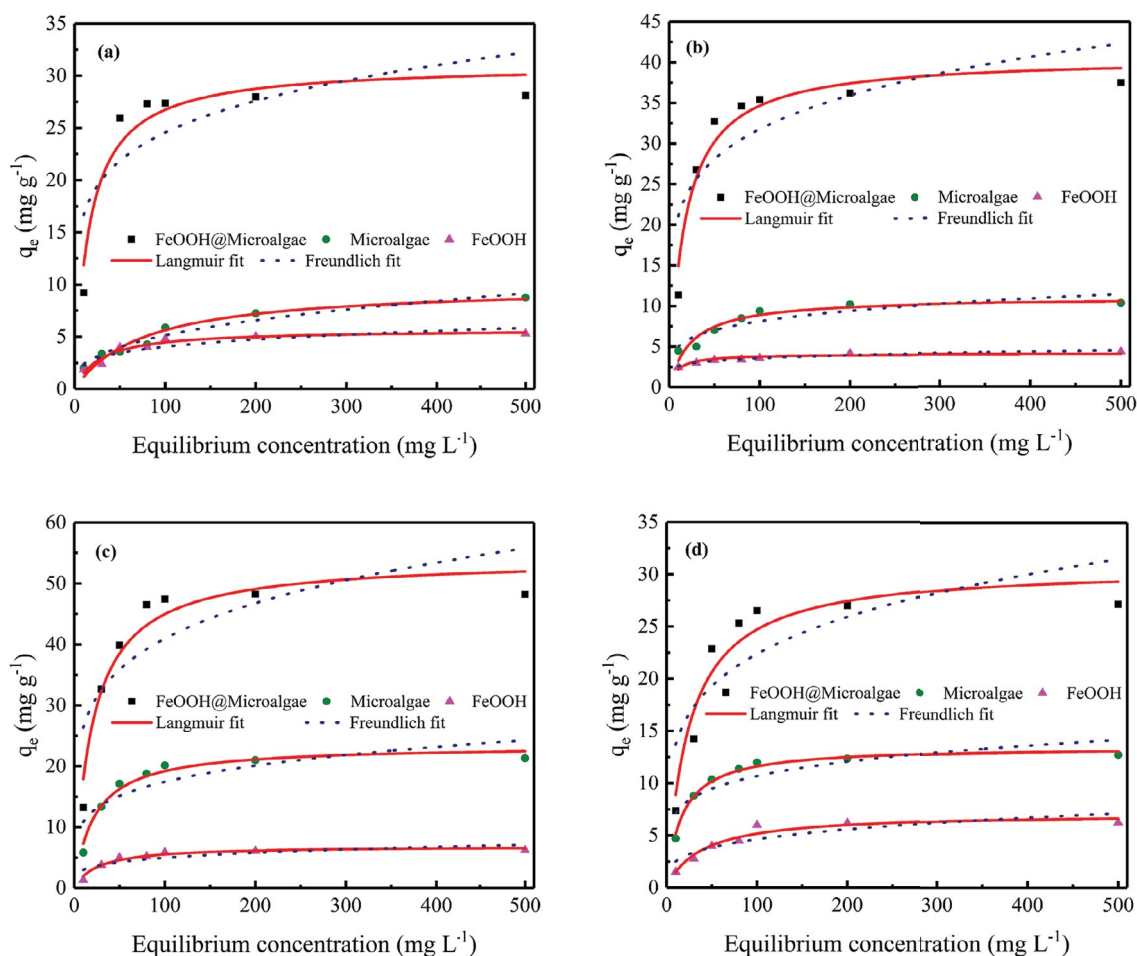


Fig. 10. Langmuir and Freundlich isotherm for (a) Cr(VI), (b) Cu(II), (c) Pb(II), and (d) Cd(II) adsorption the FeOOH@Microalgae (experiment conditions: initial Cr(VI), Cu(II), Pb(II), and Cd(II) concentration: 10–500 mg L⁻¹; adsorbent dose: 0.5 g L⁻¹; contact time: 4 h, solution pH: 3.0 for Cr(VI), Cu(II)/Pb(II)/Cd(II) for 5.3 ± 0.1; temperature: 30°C).

Furthermore, the C=C and C=O stretching vibrations of the hydrocarbon and carbonyl moieties at 1,651 cm⁻¹ on the surface of FeOOH@Microalgae were observed at 1,662; 1,659; 1,656; and 1,656 cm⁻¹. Similarly, the bending modes of aromatics have also shifted, which indicated that the process was associated with the aromatic ring. This finding was consistent with the results on microalgae immobilization by Shen et al. [111]. The wavelength variation of the characteristic peaks before and after adsorption of other adsorbents is listed in Table 6. Additionally, FeOOH@Microalgae was observed to retain most of the functional groups of the microalgae. Several functional groups, such as carboxyl (1,651 and 1,446 cm⁻¹), phosphate (1,028 cm⁻¹) and amino functional groups (3,417 and 1,540 cm⁻¹), played a major role in the adsorption process. According to this conclusion, the FeOOH@Microalgae not only had greater surface negative charge but also retained several types of functional groups. This feature enabled FeOOH@Microalgae to combine the advantages of microalgae and oxide in the adsorption process and acted as an effective adsorbent. The possible adsorption on the adsorbent may be involved in physical adsorption, complexation with functional groups, ionic exchange, surface precipitations and chemical

reaction with surface sites. Compared with the functional groups of microalgae, the functional groups of the FeOOH@Microalgae with important roles in the adsorption process, were generally similar, and the characteristic peaks were slightly shifted. Thus, the changes in the FTIR spectra confirmed the complexation of four heavy metals with functional groups in FeOOH@Microalgae.

3.3.2. SEM analysis

Fig. 13 shows SEM images and EDX spectra of FeOOH@Microalgae after adsorption of heavy metals. After adsorption of heavy metal ions, the morphology did not change significantly. However, the EDX spectrum showed that the contents of various elements have significantly changed. For FeOOH@Microalgae, the content of heavy metal ions can be ranked in the following order: Pb(II) > Cr(VI) > Cu(II) > Cd(II). The adsorption effect for Pb(II) was considerably higher than that for the other three ions, which was largely consistent with the results of previous kinetic studies. The adsorption capacity of different ions varies substantially due to the different affinities of the interaction between the surface of FeOOH@Microalgae and

Table 4
Parameters for the Langmuir and Freundlich adsorption isotherm of Cr(VI), Cu(II), Pb(II), and Cd(II)

Heavy metal	Langmuir isotherm constants			Freundlich isotherm constants		
	q_e (mg g ⁻¹)	K (L mg ⁻¹)	R_L^2	K_f (L g ⁻¹)	n	R_f^2
Cr(VI)						
FeOOH@Microalgae	31.062	0.062	0.927	11.325	5.948	0.601
Microalgae	9.906	0.013	0.942	2.799	1.001	0.953
FeOOH	5.693	0.036	0.929	4.395	1.423	0.810
Pb(II)						
FeOOH@Microalgae	54.045	0.049	0.944	16.949	5.219	0.659
Microalgae powder	23.446	0.045	0.971	6.796	4.883	0.726
Commercial FeOOH	6.912	0.039	0.954	1.794	4.517	0.712
Cu(II)						
FeOOH@Microalgae	40.625	0.058	0.948	14.008	5.622	0.663
Microalgae powder	11.024	0.042	0.901	3.099	4.772	0.829
Commercial FeOOH	4.093	0.117	0.839	1.889	7.203	0.955
Cd(II)						
FeOOH@Microalgae	30.831	0.040	0.929	8.399	4.70	0.678
Microalgae powder	13.254	0.061	0.989	4.774	5.709	0.754
Commercial FeOOH	7.154	0.026	0.946	1.361	3.750	0.787

Table 5
Comparison of Cr(VI), Cu(II), Pb(II), and Cd(II) maximum adsorption capacities of previously reported values with those of this work

Absorbent	Adsorbate	pH	Temperature (°C)	Q_m (mg g ⁻¹)	References	
FeOOH@Microalgae	Cr(VI)	3.0	30	31.06	This work	
FeOOH			25	24.5	[67]	
Oxidized carbon		2.0	20	16.26	[68]	
Unoxidized carbon		2.0	40	14.31	[68]	
Sludge-based adsorbents		2.5	25	15.3	[69]	
Iron-impregnated sorbent		5.0	40	13.72	[70]	
Mixed maghemite-magnetite nanoparticles		4.0	25	15.4	[71]	
FeOOH@Microalgae	Cu(II)	5.3	30	40.62	This work	
FeOOH			35	27.15	[64]	
Magnetic resin microspheres			5.5	25	45.80	[70]
Chloro-phosphate impregnated biochar			5.0	25	18.2	[72]
EDCMS			5.0	25	44.4	[73]
(CMC-g-CMPVA)-Fe ₃ O ₄ /SiO ₂ -NPs			5.5	25	35.3	[74]
Carboxymethylated-bacterial cellulose			4.5	25	12.63	[75]
Go-sheets-cellulose			7.0	25	25.2	[76]
Active carbon			2.1	25	6.144	[77]
Chitosan-cellulose beads			6.5	22	53.2	[78]
Crosslinked chitosan with ECH			6.0	25	35.46	[79]
Poly(vinyl pyridine ethylene glycoldimethacrylate) resin			6.0	25	18.56	[80]
Chitosan-coated sand			6.0	25	12.32	[81]
Chitosan-bound Fe ₃ O ₄ magnetic nanoparticles			5.0	27	21.5	[82]
Immobilized microorganisms on polyurethane (IPU) foam			6.0	25	28.74	[83]
Magnetic chitosan nanoparticles		5.0	35	35.5	[84]	
Bulgarian herbs		4.0	20	30.1	[85]	
Wood vinegar treated secondary compost		5.0	25	36.8	[86]	

(continued)

Table 5 Continued

Absorbent	Adsorbate	pH	Temperature (°C)	Q_m (mg g ⁻¹)	References
Xanthate-modified magnetic chitosan		5.0	25	34.5	[87]
Amino-functionalized magnetite/kaolin clay		6.0	25	16.50	[88]
Iron-coated Australian zeolite		6.5	25	9.33	[89]
Saw dust biochar		5.0	30	16.11	[90]
FeOOH@Microalgae	Pb(II)	5.3	30	54.05	This work
FeOOH			30	5.043	[66]
Barley straw		6.0	25	23.20	[91]
Rice husk		5.0	30	12.61	[92]
Activated carbon		5.0	25	15.96	[93]
Pine cone activated		5.2	25	27.53	[94]
Nano-composite cation		6.0	55	21.01	[95]
MWCNTs/ThO ₂ nanocomposite		5.5	45	30.01	[96]
Ash/nFe-A		6.0	25	588.24/833.33	[97]
Magnetic resin microspheres		5.5	25	99.19	[98]
Activated carbon		6.5	30	46.58	[99]
Active carbon		2.08	25	6.21	[77]
Crosslinked chitosan with ECH		6.0	25	34.1	[79]
Poly(vinyl pyridine-ethylene glycoldimethacrylate) resin		6.0	25	18.63	[80]
Chitosan-coated sand		6.0	25	8.18	[81]
Polyaniline grafted chitosan		6.0	30	16.07	[100]
Iron-coated Australian zeolite		6.5	25	11.16	[89]
FeOOH@Microalgae	Cd(II)	5.3	30	30.83	This work
FeOOH			6.0	20	138
Magnetic resin microspheres		5.5	25	13.75	[98]
CaTiO ₃		6.0		32.5/19.7/18.0/17.6	[101–103]
Chloro-phosphate		5.0	20	39.8	[72]
TiO ₂ /lignin		5.0	20	25.73	[104]
Magnesium oxide rice husk biochar composite		5.0	25	21.69	[105]
High-density polyethylene (HDPE) microplastics (MPs)		/	/	30.5 (ug/g)	[106]
Iron-coated Australian zeolite		6.5	25	7.24	[89]
Microplastics		6.0		0.0305	[18]
BC650		5.0	25	31.0	[107]
Nanostructure Schiff base complex based on aromatic polwyamide		7.0	30	17.42	[108]
Ternary HA/Fe–Mn oxides-loaded biochar composite		6.0	25	11.06	[109]

metal ions, which may be attributed to the complexation constant of heavy metal ions.

Fig. 14 shows the EDX-mapping before and after adsorption of Cr(VI), Cu(II), Pb(II), and Cd(II). Before adsorption, as shown in Fig. 14a, the elements Fe, C, and O mainly existed in the original FeOOH@Microalgae. After adsorption, Cr(VI), Cu(II), Pb(II), and Cd(II) was detected, which further confirmed that the Cr(VI), Cu(II), Pb(II), and Cu(II) were adsorbed on the surface of FeOOH@Microalgae. In addition, the ion distribution content was consistent with the adsorption data.

3.4. Desorption studies

The use of adsorbent in the adsorption process not only depends on the adsorption capacity but also on the reusability of the adsorbent. Generally, the excellent

regeneration of adsorbents is an important index to ensure low adsorbents costs [112–114]. To investigate the reusability of FeOOH@Microalgae, desorption experiments were performed with different desorption solutions. Fig. 15 shows the desorption efficiency of FeOOH@Microalgae in different desorption solutions, and the adsorption and desorption process of different cycle times in different desorption solutions. The results showed that the desorption efficiency of 0.01M HNO₃ was the highest, and the removal efficiency of Cr(VI) can remain over 90% after the fifth cycle. However, with an increase of the number of cycles, the removal efficiency slightly decreased, which may be attributed to the loss of adsorbents in the adsorption process and the irreversible binding between metal ions and adsorbents [115]. A similar trend was observed for the desorption of Cu(II), Pb(II), and Cd(II). After desorption of 0.01 M HCl, 0.01 M HNO₃, 0.01 M H₂SO₄, and 0.01 M HCl,

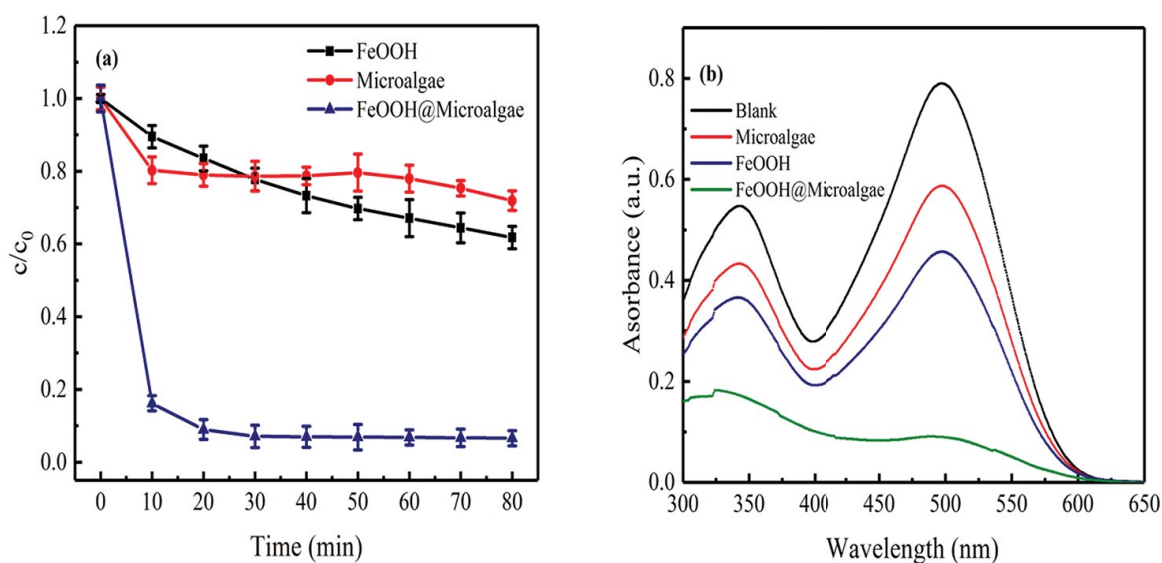


Fig. 11. (a) Adsorption efficiency of Congo red and (b) UV-vis absorption spectra of Congo red solutions treated by FeOOH@Microalgae (initial concentration of Congo red is 50 mg L^{-1}).

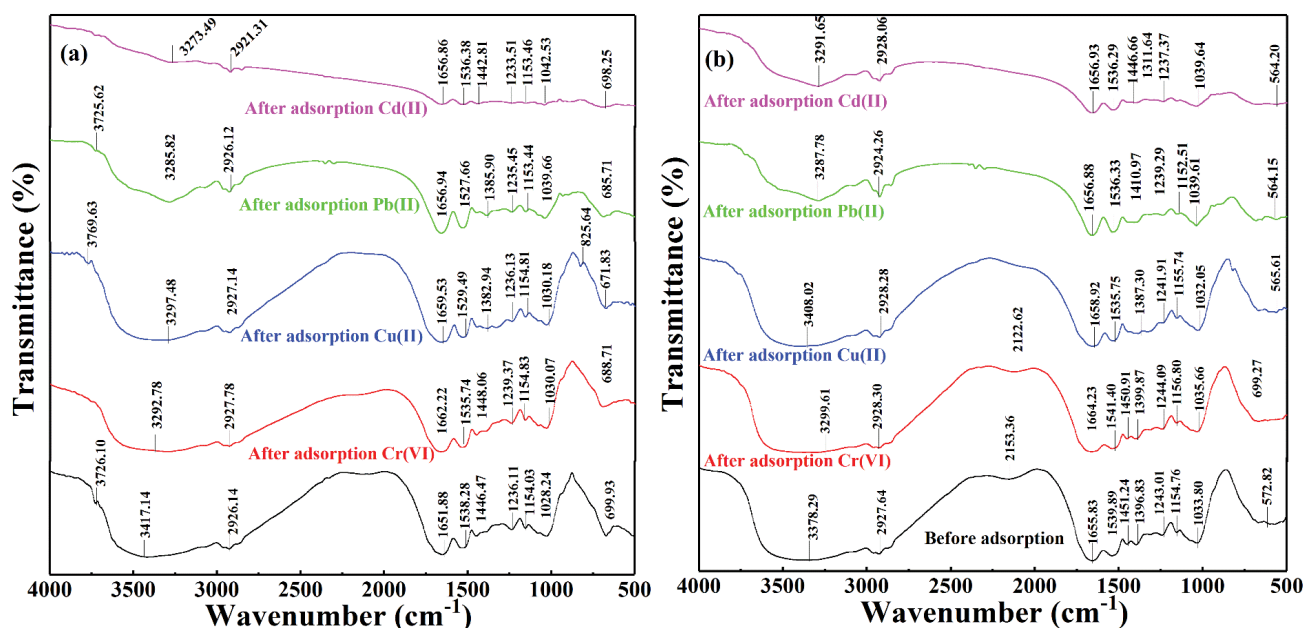


Fig. 12. FTIR spectra of the products before and after adsorption of heavy metals. (a) and (b) represent the FeOOH@Microalgae and microalgae powder.

the desorption efficiencies of Cu(II), Pb(II), and Cd(II) were higher, and the desorption trend was similar to that of Cr(VI) in the optimal desorption solution. The results indicated that FeOOH@Microalgae showed excellent reusability and metal ion removal effect and could be reused in practical application.

3.5. Practical application in wastewater

To test the environmental application of FeOOH@Microalgae, experiments were conducted on samples of heavy

metal wastewater from a factory. The 50 mg of FeOOH@Microalgae was mixed with a 50 mL wastewater sample in a 150 mL conical flask. The supernatant was separated after 60 min of adsorption; the ion concentration of the supernatant was determined using ICP. As shown in Fig. 16, FeOOH@Microalgae showed an adsorption efficiency of greater than 80% for all four ions, especially for Pb(II) (92.5%), which suggested that FeOOH@Microalgae showed good adsorption effect for wastewater treatment and hence, can be potentially employed as a highly effective adsorbent in industrial practice.

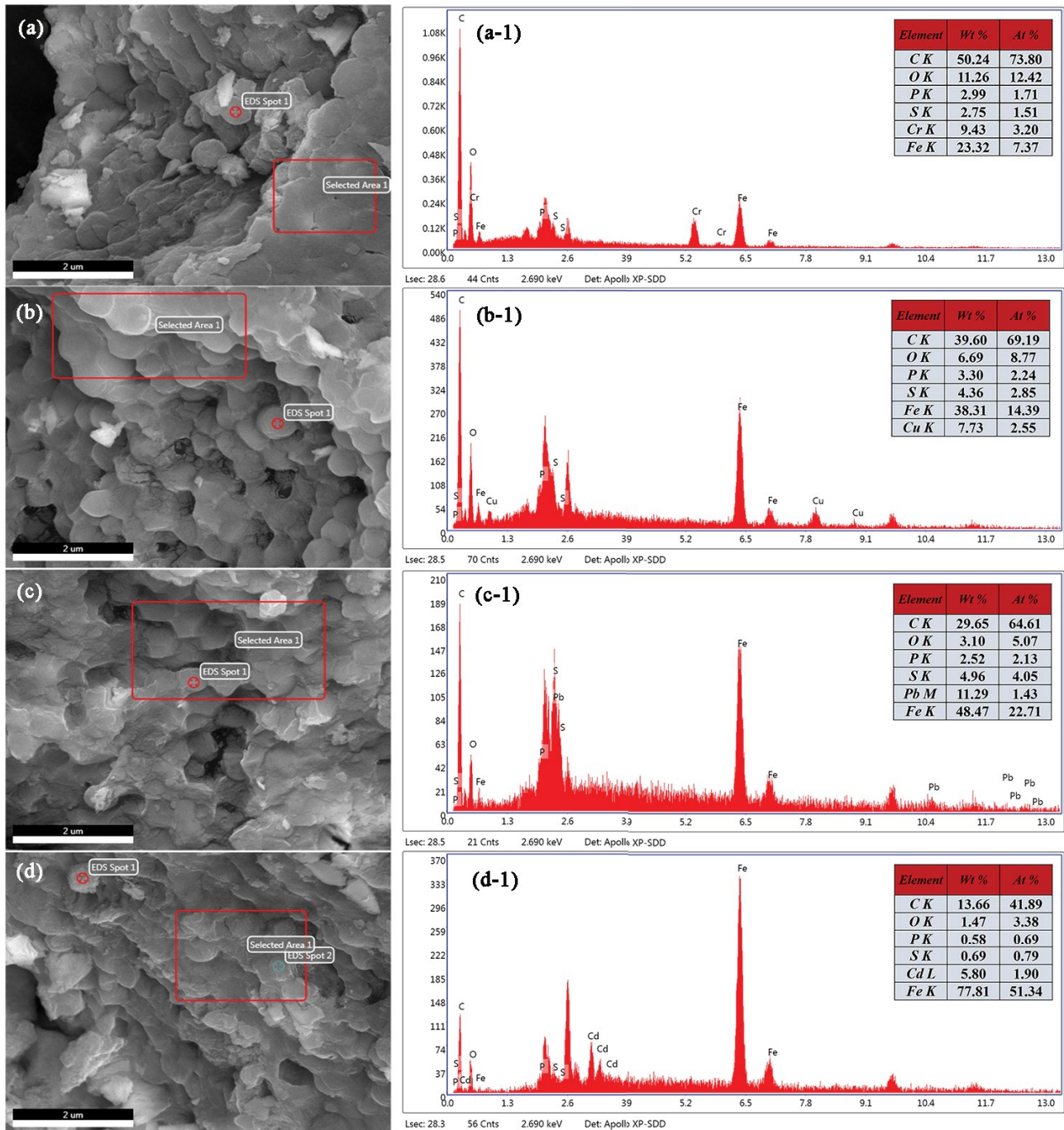


Fig. 13. (a–d) SEM images and EDX spectra of FeOOH@Microalgae after adsorption of (a-1) Cr(VI), (b-1) Cu(II), (c-1) Pb(II), and (d-1) Cd(II).

4. Conclusions

FeOOH@Microalgae, which was a composite material, was synthesized at different reaction temperatures (70°C, 60°C, and 50°C). The products combined the high adsorption property of both microalgae and FeOOH, which produced a better adsorption effect for metal ions compared with the individual use of microalgae or commercial FeOOH and traditional absorbents. The material was characterized by

XRD, FTIR, SEM, TEM, and XPS. The results indicated that microalgae were well immobilized by FeOOH, thus not only retaining the crucial functional groups of microalgae, which had a key role in adsorption, but also forming unique functional groups. According to the dynamic study, adsorption equilibrium can be reached within 180 min; the adsorption process obeyed the pseudo-second-model and the membrane diffusion process was employed as the rate control step. The sorption data fitted well with the Langmuir adsorption

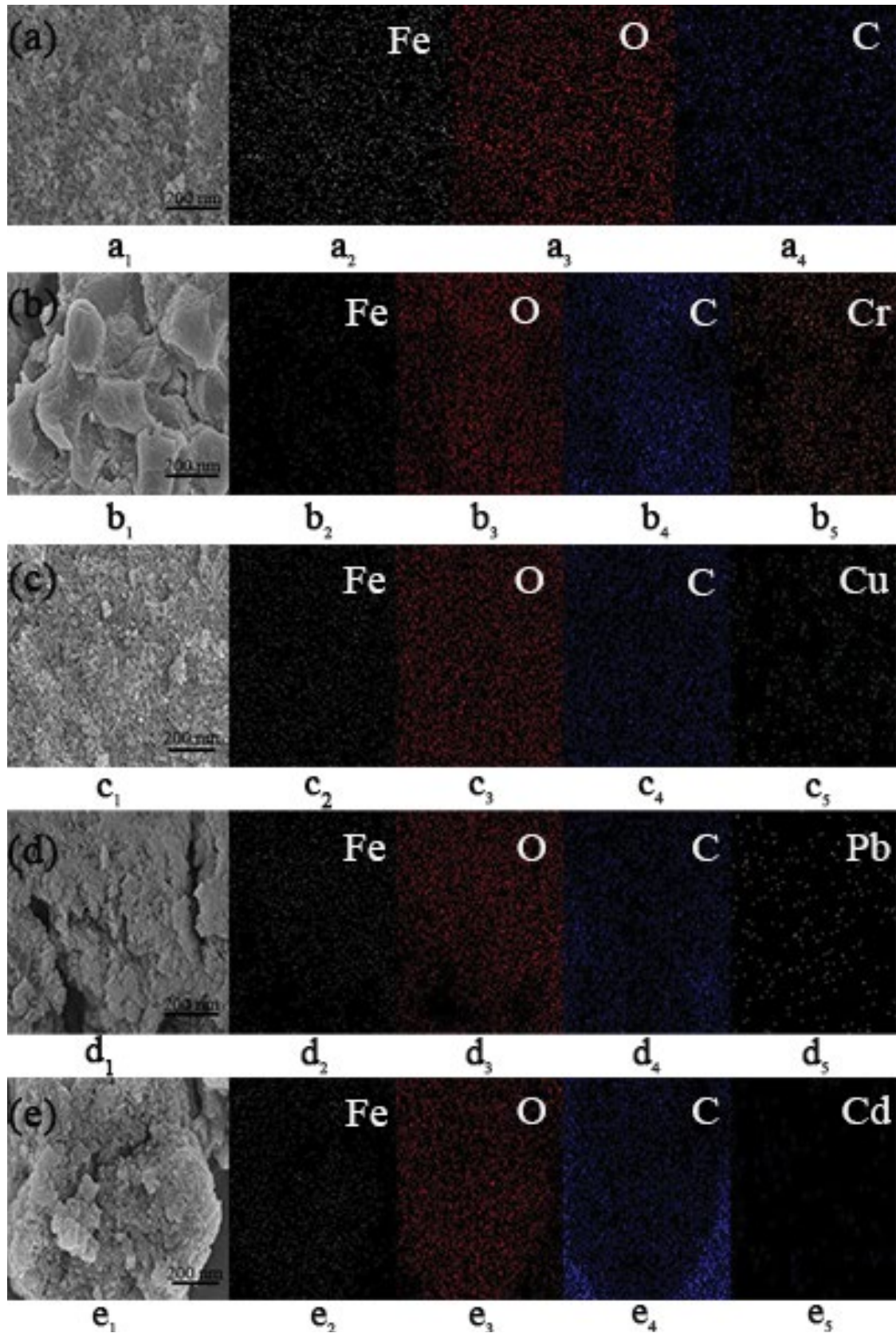


Fig. 14. SEM and EDX-mapping of (a) FeOOH@Microalgae, (b) FeOOH@Microalgae-Cr(VI), (c) FeOOH@Microalgae-Cu(II), (d) FeOOH@Microalgae-Pb(II), and (e) FeOOH@Microalgae-Cd(II).

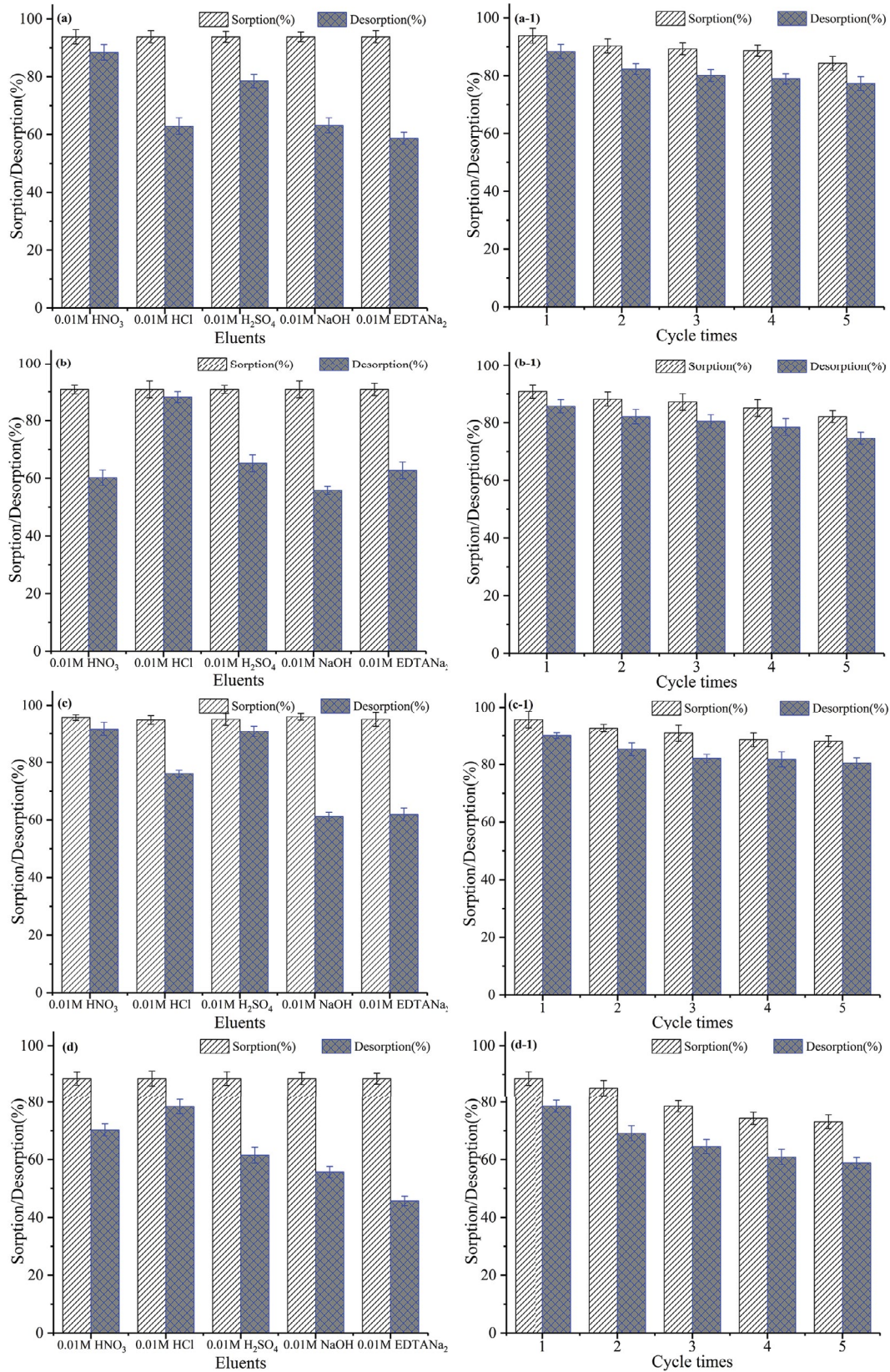


Fig. 15. Effect of different eluents on (a) Cr(VI), (b) Cu(II), (c) Pb(II), and (d) Cd(II) desorption. Adsorption–desorption cycles of (a-1) Cr(VI), (b-1) Cu(II), (c-1) Pb(II), and (d-1) Cd(II) on FeOOH@Microalgae [for Cr(VI): adsorbate concentration = 40 mg/L, pH = 3.0, desorption volume = 20 mL and for Cu(II), Pb(II), and Cd(II): adsorbate concentration = 40 mg/L, pH = 5.3, desorption volume = 20 mL].

Table 6
Comparison of the adsorption peaks in adsorbents before and after adsorption of heavy metals

Peak wavenumbers of the adsorbents	Characteristic peak wavenumbers after adsorption heavy metals			
	Cr(VI)	Cu(II)	Pb(II)	Cd(II)
FeOOH@Microalgae				
3,417	3,292	3,297	3,285	3,273
2,926	2,927	2,927	2,926	2,921
1,651	1,662	1,659	1,656	1,656
1,538	1,535	1,529	1,527	1,536
1,446	1,448	1,382	1,385	1,442
1,154	1,154	1,154	1,153	1,153
1,028	1,030	1,030	1,039	1,042
669	688	671	685	698
Microalgae				
3,378	3,299	3,408	3,287	3,291
2,927	2,928	2,928	2,924	2,928
1,655	1,664	1,658	1,656	1,656
1,539	1,541	1,535	1,536	1,536
1,451	1,450	1,442	1,443	1,446
1,396	1,399	1,387	1,395	1,311
1,243	1,244	1,241	1,239	1,237
1,154	1,156	1,155	1,152	1,155
1,033	1,035	1,032	1,039	1,039
572	699	565	564	564

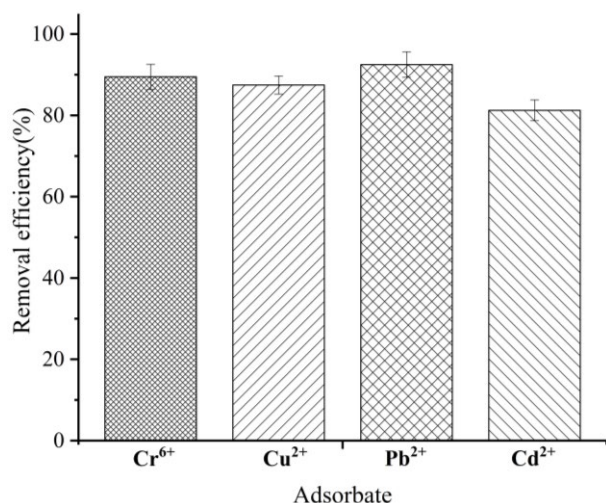


Fig. 16. Adsorption efficiency of FeOOH@Microalgae in industrial wastewater.

model; therefore, the adsorption of Cr(VI), Pb(II), Cu(II), and Cd(II) on FeOOH@Microalgae was mainly homogeneous and single-layer in nature. The maximum adsorption capacities of FeOOH@Microalgae for four metal ions were 31.06, 54.04, 40.62, and 30.83 mg g⁻¹. FeOOH@Microalgae also showed high adsorption ability for Congo red with an adsorption mechanism related to the electrostatic action

(carboxyl and hydroxyl groups binding to the metal surface), cation exchange, and complexation. These results suggested that FeOOH@Microalgae can be considered as a potential adsorbent for the removal of heavy metals and Congo red from wastewater.

Acknowledgments

This research was supported by the National Natural Science Foundation of China (No. 51604308, 31470230, 51320105006), South China Key Laboratory of Applied Microbiology Open Fund Project (SKLAM006-2018), Fundamental Research Funds for the Central Universities of Central South University (No. 2018zzts761), the Natural Science Foundation of Hunan Province (No. 2018JJ2486), Key Research and Development Projects in Hunan Province (2018WK2012), the Youth Talent Foundation of Hunan Province of China (No. 2017RS3003), and GDAS' Special Project of Science and Technology Development (2020GDASYL-20200402001).

Symbols

- q_e — Equilibrium amount adsorption capacity, mg g⁻¹
 q_t — Dynamic (at time t) amount adsorption capacity, mg g⁻¹
 k_1 — Rate constants of pseudo-first-order (min⁻¹) adsorption
 k_2 — Rate constants of pseudo-second-order (g mg⁻¹ min⁻¹) adsorption
 c_e — Equilibrium concentration of total ion in the solution, mg L⁻¹
 q_m — Maximum adsorption capacity, mg g⁻¹
 K_L — Langmuir constant
 K_F — Freundlich constant
 $1/n$ — Freundlich empirical parameter

References

- [1] M.L. Gao, Y. Zhang, X.L. Gong, Z.G. Song, Z.Y. Guo, Removal mechanism of di-n-butyl phthalate and oxytetracycline from aqueous solutions by nano-manganese dioxide modified biochar, *Environ. Sci. Pollut. Res.*, 25 (2018) 7796–7807.
- [2] J.H. Franco, B.F. da Silva, E.F.G. Dias, A.A. de Castro, T.C. Ramalho, M.V.B. Zanoni, Influence of auxochrome group in disperse dyes bearing azo groups as chromophore center in the biotransformation and molecular docking prediction by reductase enzyme: implications and assessment for environmental toxicity of xenobiotics, *Ecotoxicol. Environ. Saf.*, 160 (2018) 114–126.
- [3] Z.J. Huang, Z.Y. Huang, L.J. Feng, X.W. Luo, P.X. Wu, L.H. Cui, X.Y. Mao, Modified cellulose by polyethyleneimine and ethylenediamine with induced Cu(II) and Pb(II) adsorption potentialities, *Carbohydr. Polym.*, 202 (2018) 470–478.
- [4] Lalita, A.P. Singh, R.K. Sharma, Synthesis and characterization of graft copolymers of chitosan with NIPAM and binary monomers for removal of Cr(VI), Cu(II) and Fe(II) metal ions from aqueous solutions, *Int. J. Biol. Macromol.*, 99 (2017) 409–426.
- [5] R.L. Gao, Q.L. Fu, H.Q. Hu, Q. Wang, Y.H. Liu, J. Zhu, Highly-effective removal of Pb by co-pyrolysis biochar derived from rape straw and orthophosphate, *J. Hazard. Mater.*, 371 (2019) 191–197.
- [6] D.L. Huang, C.J. Hu, G.M. Zeng, M. Cheng, P. Xu, X.M. Gong, R.Z. Wang, W.J. Xue, Combination of Fenton processes and biotreatment for wastewater treatment and soil remediation, *Sci. Total Environ.*, 574 (2017) 1599–1610.

- [7] A.I.A. Sherlala, A.A.A. Raman, M.M. Bello, A. Asghar, A review of the applications of organo-functionalized magnetic graphene oxide nanocomposites for heavy metal adsorption, *Chemosphere*, 193 (2018) 1004–1017.
- [8] J. Barton, M.B.G. Garcia, D.H. Santos, P. Fanjul-Bolado, A. Ribotti, M. McCaul, D. Diamond, P. Magni, Screen-printed electrodes for environmental monitoring of heavy metal ions: a review, *Microchim. Acta*, 183 (2016) 503–517.
- [9] D.L. Huang, R. Deng, J. Wan, G.M. Zeng, W.J. Xue, X.F. Wen, C.Y. Zhou, L. Hu, X.G. Liu, P. Xu, X.Y. Guo, X.Y. Ren, Remediation of lead-contaminated sediment by biochar-supported nano-chlorapatite: accompanied with the change of available phosphorus and organic matters, *J. Hazard. Mater.*, 348 (2018) 109–116.
- [10] J. Ma, Y. Ma, F. Yu, X.H. Dai, Rotating magnetic field-assisted adsorption mechanism of pollutants on mechanically strong sodium alginate/graphene/l-cysteine beads in batch and fixed-bed column systems, *Environ. Sci. Technol.*, 52 (2018) 13925–13934.
- [11] C.Q. Wang, H. Wang, Pb(II) sorption from aqueous solution by novel biochar loaded with nano-particles, *Chemosphere*, 192 (2018) 1–4.
- [12] W.J. Xue, Z.W. Peng, D.L. Huang, G.M. Zeng, J. Wan, R. Xu, M. Cheng, C. Zhang, D.N. Jiang, Z.X. Hu, Nanoremediation of cadmium contaminated river sediments: microbial response and organic carbon changes, *J. Hazard. Mater.*, 359 (2018) 290–299.
- [13] S.L. Cardoso, C.S.D. Costa, E. Nishikawa, M.G.C. da Silva, M.G.A. Vieira, Biosorption of toxic metals using the alginate extraction residue from the brown algae *Sargassum filipendula* as a natural ion-exchanger, *J. Cleaner Prod.*, 165 (2017) 491–499.
- [14] R. Deng, D.L. Huang, J. Wan, W.J. Xue, L. Lei, X.F. Wen, X.G. Liu, S. Chen, Y. Yang, Z.H. Li, B. Li, Chloro-phosphate impregnated biochar prepared by co-precipitation for the lead, cadmium and copper synergic scavenging from aqueous solution, *Bioresour. Technol.*, 293 (2019) 122102.
- [15] C. Lin, W.J. Luo, T.T. Luo, Q. Zhou, H.F. Li, L.R. Jing, A study on adsorption of Cr(VI) by modified rice straw: characteristics, performances and mechanism, *J. Cleaner Prod.*, 196 (2018) 626–634.
- [16] L.E. Hernández-Hernández, A. Bonilla-Petriciolet, D.I. Mendoza-Castillo, H.E. Reynel-Ávila, Antagonistic binary adsorption of heavy metals using stratified bone char columns, *J. Mol. Liq.*, 241 (2017) 334–346.
- [17] W. Yao, J. Wang, P.Y. Wang, X.X. Wang, S.J. Yu, Y.D. Zou, J. Hou, T. Hayat, A. Alsaedi, X.K. Wang, Synergistic coagulation of GO and secondary adsorption of heavy metal ions on Ca/Al layered double hydroxides, *Environ. Pollut.*, 229 (2017) 827–836.
- [18] O. Tavakoli, V. Goodarzi, M.R. Saeb, N.M. Mahmoodi, R. Borja, Competitive removal of heavy metal ions from squid oil under isothermal condition by CR11 chelate ion exchanger, *J. Hazard. Mater.*, 334 (2017) 256–266.
- [19] Y.P. Li, Z.J. Xu, S.Y. Liu, J.W. Zhang, X.N. Yang, Molecular simulation of reverse osmosis for heavy metal ions using functionalized nanoporous graphenes, *Comput. Mater. Sci.*, 139 (2017) 65–74.
- [20] S.H. Lee, Y.G. Jeong, Y.I. Yoon, W.H. Park, Hydrolysis of oxidized polyacrylonitrile nanofibrous webs and selective adsorption of harmful heavy metal ions, *Polym. Degrad. Stab.*, 143 (2017) 207–213.
- [21] X.M. Gong, D.L. Huang, Y.G. Liu, Z.W. Peng, G.M. Zeng, P. Xu, M. Cheng, R.Z. Wang, J. Wan, Remediation of contaminated soils by biotechnology with nanomaterials: bio-behavior, applications, and perspectives, *Crit. Rev. Biotechnol.*, 38 (2018) 455–468.
- [22] G.A. Adebisi, Z.Z. Chowdhury, P.A. Alaba, Equilibrium, kinetic, and thermodynamic studies of lead ion and zinc ion adsorption from aqueous solution onto activated carbon prepared from palm oil mill effluent, *J. Cleaner Prod.*, 148 (2017) 958–968.
- [23] D. Xia, F. Tan, C.P. Zhang, X.L. Jiang, Z. Chen, H. Li, Y.M. Zheng, Q.B. Li, Y.P. Wang, ZnCl₂-activated biochar from biogas residue facilitates aqueous As(III) removal, *Appl. Surf. Sci.*, 377 (2016) 361–369.
- [24] H.T. Hao, G.F. Liu, Y.L. Wang, B.Y. Shi, K. Han, Y. Zhuang, Y. Kong, Simultaneous cationic Cu(II)-anionic Sb(III) removal by NH₂-Fe₃O₄-NTA core-shell magnetic nanoparticle sorbents synthesized via a facile one-pot approach, *J. Hazard. Mater.*, 362 (2019) 246–257.
- [25] J.W. Pan, B.Y. Gao, W. Song, X. Xu, B. Jin, Q.Y. Yue, Column adsorption and regeneration study of magnetic biopolymer resin for perchlorate removal in presence of nitrate and phosphate, *J. Cleaner Prod.*, 213 (2019) 762–775.
- [26] H.B. Li, X.L. Dong, E.B. da Silva, L.M. de Oliveira, Y.S. Chen, L.Q. Ma, Mechanisms of metal sorption by biochars: biochar characteristics and modifications, *Chemosphere*, 178 (2017) 466–478.
- [27] W.J. Xue, D.L. Huang, G.M. Zeng, J. Wan, C. Zhang, R. Xu, M. Cheng, R. Deng, Nanoscale zero-valent iron coated with rhamnolipid as an effective stabilizer for immobilization of Cd and Pb in river sediments, *J. Hazard. Mater.*, 341 (2018) 381–389.
- [28] A. Maleki, Z. Hajizadeh, V. Sharifi, Z. Emdadi, A green, porous and eco-friendly magnetic geopolymer adsorbent for heavy metals removal from aqueous solutions, *J. Cleaner Prod.*, 215 (2019) 1233–1245.
- [29] Q.Q. Yin, R.K. Wang, Z.H. Zhao, Application of Mg–Al-modified biochar for simultaneous removal of ammonium, nitrate, and phosphate from eutrophic water, *J. Cleaner Prod.*, 176 (2018) 230–240.
- [30] M. Fomina, G.M. Gadd, Biosorption: current perspectives on concept, definition and application, *Bioresour. Technol.*, 160 (2014) 3–14.
- [31] J.S. He, J.P. Chen, A comprehensive review on biosorption of heavy metals by algal biomass: materials, performances, chemistry, and modeling simulation tools, *Bioresour. Technol.*, 160 (2014) 67–78.
- [32] S.H.A. Hassan, M. Koutb, N.A. Nafady, E.A. Hassan, Potentiality of *Neopetalotriopsis clavispora* ASU1 in biosorption of cadmium and zinc, *Chemosphere*, 202 (2018) 750–756.
- [33] B.-Y. Chen, C.-Y. Chen, W.-Q. Guo, H.-W. Chang, W.-M. Chen, D.-J. Lee, C.-C. Huang, N.-Q. Ren, J.-S. Chang, Fixed-bed biosorption of cadmium using immobilized *Scenedesmus obliquus* CNW-N cells on loofa (*Luffa cylindrica*) sponge, *Bioresour. Technol.*, 160 (2014) 175–181.
- [34] S. Ozturk, B. Aslim, Z. Suludere, Cadmium(II) sequestration characteristics by two isolates of *Synechocystis* sp. in terms of exopolysaccharide (EPS) production and monomer composition, *Bioresour. Technol.*, 101 (2010) 9742–9748.
- [35] H.C. Xu, H.Y. Cai, G.H. Yu, H.L. Jiang, Insights into extracellular polymeric substances of cyanobacterium *Microcystis aeruginosa* using fractionation procedure and parallel factor analysis, *Water Res.*, 47 (2013) 2005–2014.
- [36] Z.H. Wei, R.E. Xing, X. Zhang, S. Liu, H.H. Yu, P.C. Li, Facile template-free fabrication of hollow nest-like α -Fe₂O₃ nanostructures for water treatment, *ACS Appl. Mater. Interfaces*, 5 (2012) 598–604.
- [37] X.L. Gou, G.X. Wang, X.Y. Kong, D. Wexler, J. Horvat, J. Yang, J. Park, Flutelike porous hematite nanorods and branched nanostructures: synthesis, characterisation and application for gas-sensing, *Chem. Eur. J.*, 14 (2010) 5996–6002.
- [38] E. Repo, J.K. Warchol, A. Bhatnagar, M. Sillanpää, Heavy metals adsorption by novel EDTA-modified chitosan-silica hybrid materials, *J. Colloid Interface Sci.*, 358 (2011) 261–267.
- [39] Z. Bacsik, N. Ahlsten, A. Ziadi, G.Y. Zhao, A. Garcia, B. Martin-Matute, N. Hedin, Mechanisms and kinetics for sorption of CO₂ on bicontinuous mesoporous silica modified with n-propylamine, *Langmuir*, 27 (2011) 11118–11128.
- [40] Y. Gutha, V.S. Munagapati, Removal of Pb(II) ions by using magnetic chitosan-4-((pyridin-2-ylimino)methyl) benzaldehyde Schiff's base, *Int. J. Biol. Macromol.*, 93 (2016) 408–417.
- [41] N. Zhang, G.-L. Zang, C. Shi, H.-Q. Yu, G.-P. Sheng, A novel adsorbent TEMPO-mediated oxidized cellulose nanofibrils modified with PEI: preparation, characterization, and application for Cu(II) removal, *J. Hazard. Mater.*, 316 (2016) 11–18.
- [42] X.Q. Lu, A.M. Vassallo, W.D. Johnson, Thermal stability of humic substances and their metal forms: an investigation using

- FTIR emission spectroscopy, *J. Anal. Appl. Pyrolysis*, 43 (1997) 103–113.
- [43] X.M. Ren, D.D. Shao, S.T. Yang, J. Hu, G.D. Sheng, X.L. Tan, X.K. Wang, Comparative study of Pb(II) sorption on XC-72 carbon and multi-walled carbon nanotubes from aqueous solutions, *Chem. Eng. J.*, 170 (2011) 170–177.
- [44] M. Bansal, U. Garg, D. Singh, V.K. Garg, Removal of Cr(VI) from aqueous solutions using pre-consumer processing agricultural waste: a case study of rice husk, *J. Hazard. Mater.*, 162 (2009) 312–320.
- [45] L.S. Tan, J. Xu, X.Q. Xue, Z.M. Lou, J. Zhu, S. Baig, X.H. Xu, Multifunctional nanocomposite Fe₃O₄@SiO₂-mPD/SP for selective removal of Pb(II) and Cr(VI) from aqueous solutions, *RSC Adv.*, 4 (2014) 45920–45929.
- [46] Q.M. Li, H.O. Song, R.M. Han, G.X. Wang, A.M. Li, Efficient removal of Cu(II) and citrate complexes by combined permanent magnetic resin and its mechanistic insights, *Chem. Eng. J.*, 366 (2019) 1–10.
- [47] Y.D. Zou, X.X. Wang, A. Khan, P.Y. Wang, Y.-H. Liu, A. Alsaedi, T. Hayat, X.K. Wang, Environmental remediation and application of nanoscale zero-valent iron and its composites for the removal of heavy metal ions: a review, *Environ. Sci. Technol.*, 50 (2016) 7290–7304.
- [48] Y.M. Ren, N. Li, J. Feng, T.Z. Luan, Q. Wen, Z.S. Li, M.L. Zhang, Adsorption of Pb(II) and Cu(II) from aqueous solution on magnetic porous ferrosin MnFe₂O₄, *J. Colloid Interface Sci.*, 367 (2012) 415–421.
- [49] X.Y. Guo, B. Du, Q. Wei, J. Yang, L.H. Hu, L.G. Yan, W.Y. Xu, Synthesis of amino functionalized magnetic graphenes composite material and its application to remove Cr(VI), Pb(II), Hg(II), Cd(II) and Ni(II) from contaminated water, *J. Hazard. Mater.*, 278 (2014) 211–220.
- [50] L. Sun, H.W. Yu, B. Fugetsu, Graphene oxide adsorption enhanced by in situ reduction with sodium hydrosulfite to remove acridine orange from aqueous solution, *J. Hazard. Mater.*, 203–204 (2012) 101–110.
- [51] W.S. Wan Ngah, C.S. Endud, R. Mayanar, Removal of copper(II) ions from aqueous solution onto chitosan and cross-linked chitosan beads, *React. Funct. Polym.*, 50 (2002) 181–190.
- [52] L. Zhou, Y.G. Liu, S.B. Liu, Y.C. Yin, G.M. Zeng, X.F. Tan, X. Hu, X.J. Hu, L.H. Jiang, Y. Ding, S.H. Liu, X.X. Huang, Investigation of the adsorption-reduction mechanisms of hexavalent chromium by ramie biochars of different pyrolytic temperatures, *Bioresour. Technol.*, 218 (2016) 351–359.
- [53] A. Baran, E. Biçak, Ş.H. Baysal, S. Önal, Comparative studies on the adsorption of Cr(VI) ions on to various sorbents, *Bioresour. Technol.*, 98 (2007) 661–665.
- [54] D.K. Li, Q. Li, D.Y. Mao, N.N. Bai, H.Z. Dong, A versatile bio-based material for efficiently removing toxic dyes, heavy metal ions and emulsified oil droplets from water simultaneously, *Bioresour. Technol.*, 245 (2017) 649–655.
- [55] M. Naushad, T. Ahamad, B.M. Al-Maswari, A. Abdullah Alqadami, S.M. Alshehri, Nickel ferrite bearing nitrogen-doped mesoporous carbon as efficient adsorbent for the removal of highly toxic metal ion from aqueous medium, *Chem. Eng. J.*, 330 (2017) 1351–1360.
- [56] D.K. Singh, V. Kumar, S. Mohan, S.H. Hasan, Polylysine functionalized graphene aerogel for the enhanced removal of Cr(VI) through adsorption: kinetic, isotherm, and thermodynamic modeling of the process, *J. Chem. Eng. Data*, 62 (2017) 1732–1742.
- [57] Z.Y. Li, J.Y. Chen, Y.Y. Ge, Removal of lead ion and oil droplet from aqueous solution by lignin-grafted carbon nanotubes, *Chem. Eng. J.*, 308 (2017) 809–817.
- [58] F.H. Frimmel, L. Huber, Influence of humic substances on the aquatic adsorption of heavy metals on defined mineral phases, *Environ. Int.*, 22 (1996) 507–517.
- [59] G. McKay, M.S. Otterburn, A.G. Sweeney, The removal of colour from effluent using various adsorbents—III. Silica: rate processes, *Water Res.*, 14 (1980) 15–20.
- [60] L.-S. Zhong, J.-S. Hu, H.-P. Liang, A.-M. Cao, W.-G. Song, L.-J. Wan, Self-assembled 3D flowerlike iron oxide nanostructures and their application in water treatment, *Adv. Mater.*, 18 (2006) 2426–2431.
- [61] A. Mahapatra, B.G. Mishra, G. Hota, Electrospun Fe₂O₃-Al₂O₃ nanocomposite fibers as efficient adsorbent for removal of heavy metal ions from aqueous solution, *J. Hazard. Mater.*, 258–259 (2013) 116–123.
- [62] Z.W. Wang, X.F. Zeng, X.M. Yu, H. Zhang, Z.J. Li, D. Jin, Adsorption behaviors of Cd²⁺ on Fe₂O₃/MnO₂ and the effects of coexisting ions under alkaline conditions, *Chin. J. Geochem.*, 29 (2010) 197–203.
- [63] X.L. Zhang, Q.L. Zhang, L.Q. Zhang, T. Zhang, L.Y. Hu, Particle concentration effect of Cr(VI) adsorption by Bentonite load FeOOH, *Pollut. Control Technol.*, 26 (2013) 28–32.
- [64] R. Tongyan, Study on adsorbability of Cu²⁺ by α-FeOOH nanowires, *Guangdong Chem. Ind.*, 20 (2016) 49–50.
- [65] W. Xu, H.C. Lan, H.J. Wang, H.M. Liu, J.H. Qu, Comparing the adsorption behaviors of Cd, Cu and Pb from water onto Fe-Mn binary oxide, MnO₂ and FeOOH, *Front. Environ. Sci. Eng.*, 9 (2015) 385–393.
- [66] H.W. Liu, Z.Q. Lu, H.Y. Zhang, Y.H. Chen, Y. Zhou, Adsorption performance of Aldopeda-FeOOH nanoparticles to Pb²⁺, *Inorg. Chem. Ind.*, 43 (2011) 16–18.
- [67] Y.-Y. Deng, X.-F. Xiao, D. Wang, B. Han, Y. Gao, J.-L. Xue, Adsorption of Cr(VI) from aqueous solution by ethylenediaminetetraacetic acid-chitosan-modified metal-organic framework, *J. Nanosci. Nanotechnol.*, 20 (2020) 1660–1669.
- [68] Z.A. Al-Othman, R. Ali, M. Naushad, Hexavalent chromium removal from aqueous medium by activated carbon prepared from peanut shell: adsorption kinetics, equilibrium and thermodynamic studies, *Chem. Eng. J.*, 184 (2012) 238–247.
- [69] L.G. Zhang, J.S. Pan, L. Liu, K. Song, Q.L. Wang, Combined physical and chemical activation of sludge-based adsorbent enhances Cr(VI) removal from wastewater, *J. Cleaner Prod.*, 238 (2019) 117904.
- [70] Y.N. Zhu, H. Zhang, H. Zeng, M. Liang, R. Lu, Adsorption of chromium(VI) from aqueous solution by the iron(III)-impregnated sorbent prepared from sugarcane bagasse, *Int. J. Environ. Sci. Technol.*, 9 (2012) 463–472.
- [71] S.R. Chowdhury, E.K. Yanful, A.R. Pratt, Chemical states in XPS and Raman analysis during removal of Cr(VI) from contaminated water by mixed maghemite-magnetite nanoparticles, *J. Hazard. Mater.*, 235–236 (2012) 246–256.
- [72] S.-J. Lee, J.H. Park, Y.-T. Ahn, J.W. Chung, Comparison of heavy metal adsorption by peat moss and peat moss-derived biochar produced under different carbonization conditions, *Water Air Soil Pollut.*, 226 (2015) 1–11.
- [73] Y. Ren, H.A. Abbood, F.B. He, H. Peng, K.X. Huang, Magnetic EDTA-modified chitosan/SiO₂/Fe₃O₄ adsorbent: preparation, characterization, and application in heavy metal adsorption, *Chem. Eng. J.*, 226 (2013) 300–311.
- [74] N.A. Dahlan, A.K. Veeramachineni, S.J. Langford, J. Pushpamalar, Developing of a magnetite film of carboxymethyl cellulose grafted carboxymethyl polyvinyl alcohol (CMC-g-CMPVA) for copper removal, *Carbohydr. Polym.*, 173 (2017) 619–630.
- [75] S.Y. Chen, Y. Zou, Z.Y. Yan, W. Shen, S.K. Shi, X. Zhang, H.P. Wang, Carboxymethylated-bacterial cellulose for copper and lead ion removal, *J. Hazard. Mater.*, 161 (2009) 1355–1359.
- [76] A.A. Yakout, R.H. El-Sokkary, M.A. Shreadah, O.G. Abdel Hamid, Cross-linked graphene oxide sheets via modified extracted cellulose with high metal adsorption, *Carbohydr. Polym.*, 172 (2017) 20–27.
- [77] S.-F. Lo, S.-Y. Wang, M.-J. Tsai, L.-D. Lin, Adsorption capacity and removal efficiency of heavy metal ions by Moso and Ma bamboo activated carbons, *Chem. Eng. Res. Des.*, 90 (2012) 1397–1406.
- [78] N. Li, R.B. Bai, Copper adsorption on chitosan-cellulose hydrogel beads: behaviors and mechanisms, *Sep. Purif. Technol.*, 42 (2005) 237–247.
- [79] A.-H. Chen, S.-C. Liu, C.-Y. Chen, C.-Y. Chen, Comparative adsorption of Cu(II), Zn(II), and Pb(II) ions in aqueous solution

- on the crosslinked chitosan with epichlorohydrin, *J. Hazard. Mater.*, 154 (2008) 184–191.
- [80] A. Duran, M. Soylak, S.A. Tuncel, Poly(vinyl pyridine-poly ethylene glycol methacrylate-ethylene glycol dimethacrylate) beads for heavy metal removal, *J. Hazard. Mater.*, 155 (2008) 114–120.
- [81] M.-W. Wan, C.-C. Kan, B.D. Rogel, M.L.P. Dalida, Adsorption of copper (II) and lead (II) ions from aqueous solution on chitosan-coated sand, *Carbohydr. Polym.*, 80 (2010) 891–899.
- [82] Y.-C. Chang, D.-H. Chen, Preparation of adsorption properties of monodisperse chitosan-bound Fe_3O_4 magnetic nanoparticles for removal of Cu(II) ions, *J. Colloid Interface Sci.*, 283 (2005) 446–451.
- [83] L.-C. Zhou, Y.-F. Li, X. Bai, G.-H. Zhao, Use of microorganisms immobilized on composite polyurethane foam to remove Cu(II) from aqueous solution, *J. Hazard. Mater.*, 167 (2009) 1106–1113.
- [84] Y.W. Chen, J.L. Wang, Preparation and characterization of magnetic chitosan nanoparticles and its application for Cu(II) removal, *Chem. Eng. J.*, 168 (2011) 286–292.
- [85] L.P. Ivanova, A.K. Detcheva, P.S. Vassileva, Characterization of two Bulgarian herbs for use as biosorbents for Copper(II), *Anal. Lett.*, 52 (2019) 2650–2662.
- [86] L. Liu, X.P. Guo, S.Q. Wang, L. Li, Y. Zeng, G.H. Liu, Effects of wood vinegar on properties and mechanism of heavy metal competitive adsorption on secondary fermentation based composites, *Ecotoxicol. Environ. Saf.*, 150 (2018) 270–279.
- [87] Y.H. Zhu, J. Hu, J.L. Wang, Competitive adsorption of Pb(II), Cu(II) and Zn(II) onto xanthate-modified magnetic chitosan, *J. Hazard. Mater.*, 221–222 (2012) 155–161.
- [88] L.L. Qin, L.G. Yan, J. Chen, T.T. Liu, H.Q. Yu, B. Du, Enhanced removal of Pb^{2+} , Cu^{2+} , and Cd^{2+} by amino-functionalized magnetite/kaolin clay, *Ind. Eng. Chem. Res.*, 55 (2016) 7344–7354.
- [89] T.C. Nguyen, P. Loganathan, T.V. Nguyen, S. Vigneswaran, J. Kandasamy, R. Naidu, Simultaneous adsorption of Cd, Cr, Cu, Pb, and Zn by an iron-coated Australian zeolite in batch and fixed-bed column studies, *Chem. Eng. J.*, 270 (2015) 393–404.
- [91] G.-X. Yang, H. Jiang, Amino modification of biochar for enhanced adsorption of copper ions from synthetic wastewater, *Water Res.*, 48 (2014) 396–405.
- [91] E. Pehlivan, T. Altun, S. Parlayıcı, Utilization of barley straws as biosorbents for Cu^{2+} and Pb^{2+} ions, *J. Hazard. Mater.*, 164 (2009) 982–986.
- [92] Q.G. Feng, Q.Y. Lin, F.Z. Gong, S. Sugita, M. Shoya, Adsorption of lead and mercury by rice husk ash, *J. Colloid Interface Sci.*, 278 (2004) 1–8.
- [93] T. Depci, A.R. Kul, Y. Önal, Competitive adsorption of lead and zinc from aqueous solution on activated carbon prepared from Van apple pulp: study in single- and multi-solute systems, *Chem. Eng. J.*, 200–202 (2012) 224–236.
- [94] M. Momčilović, M. Purenović, A. Bojić, A. Zarubica, M. Randelović, Removal of lead(II) ions from aqueous solutions by adsorption onto pine cone activated carbon, *Desalination*, 276 (2011) 53–59.
- [95] M. Naushad, Surfactant assisted nano-composite cation exchanger: development, characterization and applications for the removal of toxic Pb^{2+} from aqueous medium, *Chem. Eng. J.*, 235 (2014) 100–108.
- [96] A. Mittal, M. Naushad, G. Sharma, Z.A. Allothman, S.M. Wabaidur, M. Alam, Fabrication of MWCNTs/ ThO_2 nanocomposite and its adsorption behavior for the removal of Pb(II) metal from aqueous medium, *Desal. Water. Treat.*, 57 (2016) 21863–21869.
- [97] M. Ghasemi, M. Naushad, N. Ghasemi, Y. Khosravi-fard, Adsorption of Pb(II) from aqueous solution using new adsorbents prepared from agricultural waste: adsorption isotherm and kinetic studies, *J. Ind. Eng. Chem.*, 20 (2014) 2193–2199.
- [98] Z.X. Li, Z.H. Wang, C.T. Wang, S.L. Ding, F.W. Li, H.F. Lin, Preparation of magnetic resin microspheres M-P(MMA-DVB-GMA) and the adsorption property to heavy metal ions, *Appl. Surf. Sci.*, 496 (2019) 143708.
- [99] K.A. Krishnan, A. Sheela, T.S. Anirudhan, Kinetic and equilibrium modeling of liquid-phase adsorption of lead and lead chelates on activated carbons, *J. Chem. Technol. Biotechnol.*, 78 (2003) 642–653.
- [100] R. Karthik, S. Meenakshi, Removal of Pb(II) and Cd(II) ions from aqueous solution using polyaniline grafted chitosan, *Chem. Eng. J.*, 263 (2015) 168–177.
- [101] D. Zhang, P. Yu, X. He, Preparation and characterization of porous calcium titanate-based coated glass fiber filter material and its application in determination of lead and cadmium ion concentrations in water, *J. AOAC Int.*, 94 (2011) 1925–1933.
- [102] D. Zhang, C.-L. Zhang, P. Zhou, Preparation of porous nano-calcium titanate microspheres and its adsorption behavior for heavy metal ion in water, *J. Hazard. Mater.*, 186 (2011) 971–977.
- [103] D. Zhang, P. Hou, Preparation of nano-calcium titanate powder and its adsorption behavior for lead ion and cadmium ion in water, *Acta Chim. Sinica*, 67 (2009) 1336–1342.
- [104] Ł. Klapiszewski, K. Siwińska-Stefańska, D. Kołodyńska, Development of lignin based multifunctional hybrid materials for Cu(II) and Cd(II) removal from the aqueous system, *Chem. Eng. J.*, 330 (2017) 518–530.
- [105] J.X. Xiang, Q.T. Lin, S.L. Cheng, J.L. Guo, X.S. Yao, Q.J. Liu, G.C. Yin, D.F. Liu, Enhanced adsorption of Cd(II) from aqueous solution by a magnesium oxide-rice husk biochar composite, *Environ. Sci. Pollut. Res.*, 25 (2018) 14032–14042.
- [106] F.Y. Wang, W.W. Yang, P. Cheng, S.Q. Zhang, S.W. Zhang, W.T. Jiao, Y.H. Sun, Adsorption characteristics of cadmium onto microplastics from aqueous solutions, *Chemosphere*, 235 (2019) 1073–1080.
- [107] R.H. Chang, S.P. Sohi, F.Q. Jing, Y.Y. Liu, J.W. Chen, A comparative study on biochar properties and Cd adsorption behavior under effects of ageing processes of leaching, acidification and oxidation, *Environ. Pollut.*, 254 (2019) 113123.
- [108] M. Aghaei, A.H. Kianfar, M. Dinari, Green synthesis of nano-structure Schiff base complex based on aromatic polyamide and manganese(III) for elimination of Hg(II) and Cd(II) from solutions, *J. Chem. Soc.*, 16 (2019) 2489–2500.
- [109] J.H. Guo, C.Z. Yan, Z.X. Luo, H.D. Fang, S.G. Hu, Y.L. Cao, Synthesis of a novel ternary HA/Fe-Mn oxides-loaded biochar composite and its application in cadmium(II) and arsenic(V) adsorption, *J. Environ. Sci.*, 85 (2019) 168–176.
- [110] B. Wang, H.B. Wu, L. Yu, R. Xu, L. Teik-Thye, X.W.(D). Lou, Template-free formation of uniform urchin-like $\alpha\text{-FeOOH}$ hollow spheres with superior capability for water treatment, *Adv. Mater.*, 24 (2012) 1111–1116.
- [111] Y. Shen, H. Li, W.Z. Zhu, S.-H. Ho, W.Q. Yuan, J.F. Chen, Y.P. Xie, Microalgal-biochar immobilized complex: a novel efficient biosorbent for cadmium removal from aqueous solution, *Bioresour. Technol.*, 244 (2017) 1031–1038.
- [112] J.K. Bediako, W. Wei, S. Kim, Y.-S. Yun, Removal of heavy metals from aqueous phases using chemically modified waste Lyocell fiber, *J. Hazard. Mater.*, 299 (2015) 550–561.
- [113] Z.L. Du, T. Zheng, P. Wang, L.L. Hao, Y.X. Wang, Fast microwave-assisted preparation of a low-cost and recyclable carboxyl modified lignocellulose-biomass jute fiber for enhanced heavy metal removal from water, *Bioresour. Technol.*, 201 (2016) 41–49.
- [114] H.J. Dai, Y. Huang, H.H. Huang, Eco-friendly polyvinyl alcohol/carboxymethyl cellulose hydrogels reinforced with graphene oxide and bentonite for enhanced adsorption of methylene blue, *Carbohydr. Polym.*, 185 (2018) 1–11.
- [115] Y.K. Long, L. Xiao, Q.H. Cao, Co-polymerization of catechol and polyethylenimine on magnetic nanoparticles for efficient selective removal of anionic dyes from water, *Powder Technol.*, 310 (2017) 24–34.